

Ranking Perspective for Tree-based Methods with Applications to Symbolic Feature Selection

Hengrui Luo

*Lawrence Berkeley National Laboratory
Berkeley, CA, 94720, USA
Department of Statistics, Rice University
Houston, TX, 77005, USA*

HRLUO@RICE.EDU

Meng Li

*Department of Statistics
Department of Statistics, Rice University
Houston, TX 77005, USA*

MENG@RICE.EDU

Abstract

Tree-based methods are powerful nonparametric techniques in statistics and machine learning. However, their effectiveness, particularly in finite-sample settings, is not fully understood. Recent applications have revealed their surprising ability to distinguish transformations (which we call *symbolic feature selection*) that remain obscure under current theoretical understanding. This work provides a finite-sample analysis of tree-based methods from a ranking perspective. We link oracle partitions in tree methods to response rankings at local splits, offering new insights into their finite-sample behavior in regression and feature selection tasks. Building on this local ranking perspective, we extend our analysis in two ways: (i) We examine the global ranking performance of individual trees and ensembles, including Classification and Regression Trees (CART) and Bayesian Additive Regression Trees (BART), providing finite-sample oracle bounds, ranking consistency, and posterior contraction results. (ii) Inspired by the ranking perspective, we propose concordant divergence statistics \mathcal{T}_0 to evaluate symbolic feature mappings and establish their properties. Numerical experiments demonstrate the competitive performance of these statistics in symbolic feature selection tasks compared to existing methods.

Keywords: Symbolic regressions, ranking models, Bayesian regression trees.

1 Introduction

1.1 Tree regressions

Tree-based methods, including CART (Breiman et al., 1987; Agarwal et al., 2022), Bayesian CART (Chipman et al., 1998), and their ensembles such as random forests (Hastie et al., 2009) and Bayesian additive regression trees (BART Chipman et al. (2010)), are popular nonparametric techniques in statistics and machine learning (Breiman et al., 1987; Hastie et al., 2009). These tree-based methods are highly effective in practice, showing competitive performance in wide-ranging tasks such as regression (Grinsztajn et al., 2022; Luo and Pratola, 2023; Luo et al., 2024), classification (Yichen Zhu and Dunson, 2023), causal inference (Hahn et al., 2020), and feature selection (Bleich et al., 2014). Their empirical success has motivated a growing literature that aims to provide theoretical guarantees (Linero, 2018; Athey et al.; Ročková and van der Pas, 2020; Ronen et al., 2022). However, much of this research relies on asymptotic analysis, and finite-sample understanding, which directly addresses observed empirical effectiveness, remains limited.

In addition, some of their recent applications in interpretable machine learning show success beyond the reach of current theoretic understanding. In particular, Ye et al. (2024) has proposed the use of BART to achieve effective and scalable regression tools for symbolic regression, a rapidly

developing field that seeks to identify the nonlinear dependence between data from a given set of mathematical expressions (Makke and Chawla, 2024). The authors show empirical evidence that BART is able to distinguish transformations of the same active variable with a small sample size, which is a crucial property to ensure accurate performance of a nonparametric variable selection method in symbolic regression. The existing statistical literature has a limited scope to decipher this property as the relevance of transformations of the same active variable is invariant from a traditional nonparametric variable selection perspective.

In this article, we attempt to offer new insights from ranking perspective in the current paper and propose a new divergence based on this perspective. We address the challenges above by connecting tree-based methods with ranking (Cl emen on and Robbiano, 2015; Cl emen on and Vogel, 2019), which is an underdeveloped perspective in the literature on feature selection. This connection is inherently within the finite-sample regime. It leads to conceptual elucidation of a class of tree-based methods, and additionally motivates new statistics that are particularly useful for screening transformations in symbolic regression. Our finite-sample connection is broadly applicable to Bayesian and non-Bayesian tree-based methods. We also establish asymptotic theory by connecting BART with ranking.

Following the background introduced in Section 1, the rest of the paper is organized as follows: Section 2 introduces the notations, concept of trees, and the principal decision ratios, around which we organized our discussions. Section 3 analyzes the oracle partition, refines per-node analysis along a single tree and discusses the feature selection behavior when we only consider local splits on univariate input variables. Section 4 furthers our discussions from the behavior of local splits to the behavior of global regression using CART and BART with a focus on ranking. Section 5 introduces a novel divergence statistics \mathcal{T}_0 inspired by the local splits studied. Section 6 provides experimental evidence showing that our theoretical analysis and \mathcal{T}_0 results match the BART symbolic feature selection on synthetic datasets. Section 7 concludes the paper and outlines several directions for future research.

1.2 Tree methods for variable selections

Variable importance is crucial for identifying significant features. Tree-based methods, such as CART and BART, have significantly advanced variable and feature selection (Linerio, 2018; Breiman et al., 1987; Bleich et al., 2014). They provide robust mechanisms for assessing variable importance and operational selection. Random forests are also widely used for this purpose through various mechanisms. A foundational work applied random forests to microarray data for gene selection, demonstrating the method’s accuracy in identifying relevant genes, outperforming other techniques (D iaz-Uriarte and De Andr es, 2006).

On one hand, random forests can produce variable importance indices for variable and model selections (Genuer et al., 2010). For example, the ranger implementation optimized random forests for high-dimensional data and large-scale applications (Wright and Ziegler, 2017), which provides measures of variable importance from the random forest. These measures indicate the significance of each feature in predicting the response variable. To address biases in random forests especially with correlated predictors (Strobl et al., 2008), instead of permuting values unconditionally, the values are permuted conditionally based on the values of other variables.

Operational selection can be achieved during dynamic growth of the tree and involves actively choosing variables based on specific criteria. For example, the Boruta method (Kursa and Rudnicki, 2010) uses random forests for the selection of all relevant characteristics by comparing the original attributes with the randomized counterparts, ensuring that all relevant characteristics are retained. On the other hand, BART captures the uncertainty in variable importance, leading to more accurate

models, particularly in gene regulation studies (Horiguchi et al., 2021) but also induces variable importance for selection (Bleich et al., 2014).

1.3 Tree-based rankings

Cl emen on et al. (2011) explored adaptive partitioning schemes for bipartite ranking, showing how decision trees can create adaptive partitions to improve ranking performance. These schemes dynamically adjust tree partitions to better capture the distribution of positive and negative classes. Adaptive partitioning uses decision trees to refine partitions based on ranking performance feedback. Their TreeRank method adapts the tree structure to split nodes to improve the AUC of ROC. It is useful for complex data distributions that require flexible partitioning. Furthermore, TreeRank Tournament algorithm (Cl emen on and Robbiano, 2015) enhances this by integrating multiple trees, stabilizing ranking performance, and extends its capability in feature selection.

Cl emen on and Vayatis (2009) examined partitioning rules for bipartite ranking, highlighting the role of decision tree methods in creating effective partitions to approximate the optimal ROC curve. They showed that tree-based partitioning rules could be optimized to improve ranking by focusing on informative splits that maximize class separation. CART variants and other decision tree methods are essential for statistical ranking problems, including bipartite ranking (Menon and Williamson, 2016; Uematsu and Lee, 2017).

Beyond bipartite ranking, a scoring function can be estimated from leaf nodes of a CART or other regression model (Cossock and Zhang, 2006). When an instance is classified into a leaf node, the score of that leaf node serves as the estimated score for the instance. This approach transforms the tree model into a scoring function that can be used for ranking purposes, which we will revisit in Section 4.

2 Oracle Partitions

2.1 Notation

We consider the regression problem and the following data generating model:

$$y_i = f(\mathbf{x}_i) + \epsilon_i, \quad i = 1, 2, \dots, N, \quad (1)$$

$$\epsilon_i \sim N(0, \sigma_\epsilon^2)$$

$$\mathbf{z}_i = (\theta_1 \mathbf{x}_i, \dots, \theta_q \mathbf{x}_i) \in \mathbb{R}^q, \quad (2)$$

with continuous covariates variables $\mathbf{x}_i \in \mathbb{R}^d$ and their transformed symbolic features $\mathbf{z}_i \in \mathbb{R}^q$ under a collection of feature mappings $\theta_\bullet : \mathbb{R}^d \rightarrow \mathbb{R}$. This collection of feature mappings $\theta_1, \dots, \theta_q$ is usually constructed and selected by symbolic regressions (e.g., sin, cos, exp), to approximate continuous responses $y_i \in \mathbb{R}$. When $q = d$ and $\theta_i = \pi_i$ (i.e., projection onto the i -th coordinate) (1) reduces to the usual regression setting of $y_i = f(\mathbf{x}_i) + \epsilon_i$. In other words, the feature mappings $\theta_1, \dots, \theta_q$ allow us to consider a more general regression setting by sending the data matrix into the following feature matrix

$$\begin{pmatrix} \mathbf{x}_1 \\ \vdots \\ \mathbf{x}_N \end{pmatrix} \in \mathbb{R}^{N \times d} \mapsto \begin{pmatrix} \theta_1 \mathbf{x}_1, & \dots, & \theta_q \mathbf{x}_1 \\ \vdots & & \vdots \\ \theta_1 \mathbf{x}_N, & \dots, & \theta_q \mathbf{x}_N \end{pmatrix} = \begin{pmatrix} \mathbf{z}_1 \\ \vdots \\ \mathbf{z}_N \end{pmatrix} \in \mathbb{R}^{N \times q}.$$

We shall distinguish \mathbf{x}_i and \mathbf{z}_i by referring to \mathbf{x}_i as *inputs* and \mathbf{z}_i as *features* or *predictors*. The population counterpart of the model above omits the index i in the notation when we do not need to refer to each sample.

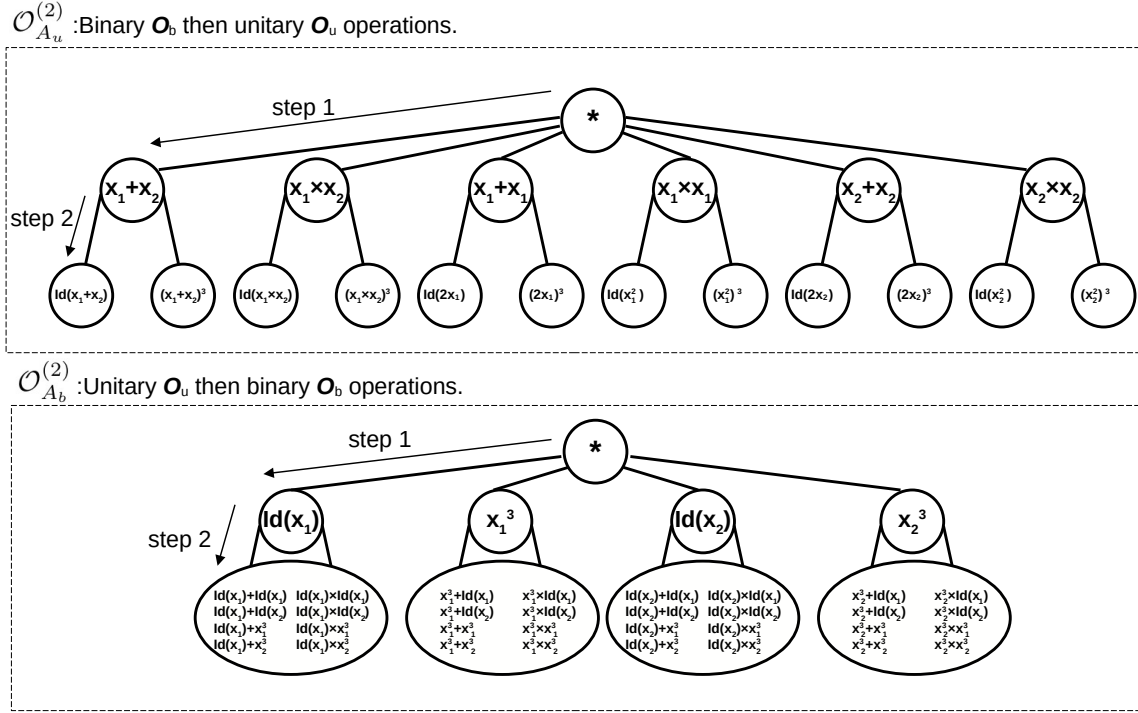


Figure 1: We illustrate 2-layer symbolic regression with $\mathcal{O}_u = \{id, x^3\}$ and $\mathcal{O}_b = \{+, \times\}$. We also follow the notation convention $\mathcal{O}_{A_u}^{(2)}$ and $\mathcal{O}_{A_b}^{(2)}$ for the architectures specified in Ye et al. (2024). We displayed all of the possible features in a 2-step symbolic composition using tree structure, showing the rapidly increasing number q of features, namely transformed symbolic feature z 's.

Example 1 (Symbolic feature mappings) Consider $d = 2$ and input variable $\mathbf{x} = (x_1, x_2) \in \mathbb{R}^2$ and an operator set $\mathcal{O}_b = \{+, \times\}$, in one step composition there are $q = 2 \times 2 \times 2 = 8$ features (i.e., combinations $\{x_1, x_2\} \otimes \{+, \times\} \otimes \{x_1, x_2\}$) $z_1 = 2x_1, z_2 = x_1 + x_2, \dots, z_8 = x_2^2$ (but only 6 distinct features as shown in Figure 1); suppose the next step we have an operator set $\mathcal{O}_u = \{id, x^3\}$ then in one step composition there are $q = 6 \times 2 = 12$ different features. Even with only two composition steps, the dimensionality q of features grows quickly (Bryant, 1992). Due to repetitive use of this composition construction in symbolic regression, $q \gg d$ and these q features are usually highly correlated, making feature (pre-)selection necessary in symbolic regressions.

In Ye et al. (2024), BART is applied to perform feature selection among all these symbolic features (which are highly correlated, and identical if noiseless composition is assumed) and achieve good performance from the corresponding symbolic regression model using the chosen features. If we take different orders of compositions (i.e., taking unitary operation first, denoted as $\mathcal{O}_{A_u}^{(2)}$; or taking binary operation first, denoted as $\mathcal{O}_{A_b}^{(2)}$), the number of features will change.

Although we assume additive noises ϵ_i such that $\mathbb{E}\epsilon_i = 0$ and $\text{Var}(\epsilon_i) = \sigma_\epsilon^2 > 0$, the ranking perspective studied in this article also covers the noise-free setting with $\sigma_\epsilon^2 = 0$. We denote the pairs of observations as

$$\begin{aligned} \mathcal{X}^{(N)} &= \{\mathbf{x}_1, \mathbf{x}_2, \dots, \mathbf{x}_N\} = \{(\mathbf{x}_{1,1}, \dots, \mathbf{x}_{1,d}), (\mathbf{x}_{2,1}, \dots, \mathbf{x}_{2,d}), \dots, (\mathbf{x}_{N,1}, \dots, \mathbf{x}_{N,d})\}, \\ \mathcal{Z}^{(N)} &= \{z_1, z_2, \dots, z_N\}, \quad \mathcal{Y}^{(N)} = \{y_1, y_2, \dots, y_N\}. \end{aligned}$$

We use an enclosing round bracket when the observation pairs are sorted according to the ranks of response y 's, i.e.,

$$(\mathbf{z}_{(1)}, y_{(1)}), (\mathbf{z}_{(2)}, y_{(2)}), \dots, (\mathbf{z}_{(N)}, y_{(N)}), \quad (3)$$

$$\text{or } (\mathbf{x}_{(1)}, y_{(1)}), (\mathbf{x}_{(2)}, y_{(2)}), \dots, (\mathbf{x}_{(N)}, y_{(N)}), \quad (4)$$

where $y_{(1)} < y_{(2)} < \dots < y_{(N)}$; here $\mathbf{x}_{(i)} = (\mathbf{x}_{(i),1}, \mathbf{x}_{(i),2}, \dots, \mathbf{x}_{(i),d})$ when written in the form of each coordinate, and likewise $\mathbf{z}_{(i)} = (\mathbf{z}_{(i),1}, \mathbf{z}_{(i),2}, \dots, \mathbf{z}_{(i),q})$. We assume that there are no ties among the responses throughout the paper.

2.2 Recursive partition in tree-based models

A binary tree divides the predictor space and consists of internal nodes and leaf nodes. The leaf nodes form a partition of the predictor space; for a tree \mathcal{T} consisting of K leaf nodes, the conditional mean of the response $\mathbb{E}(y \mid \mathbf{x}) = g(\mathbf{x}) = \sum_{i=1}^K \mu_i \mathbf{1}(\mathbf{x} \in P_i \mid \mathcal{T})$, where $\mu_i \in \mathbb{R}$ is the mean value associated with the i th leaf node P_i for $i = 1, \dots, K$.

To recursively construct binary trees (Quinlan, 1986; Breiman et al., 1987; Hastie et al., 2009), we can split at each node by splitting coordinates and splitting values (a.k.a., cutoff values); in particular, for an internal node η with split parameters (C_η, k_η) , we divide η into the left and right child nodes $\mathbf{x}_{\bullet, k_\eta} \leq C_\eta$ and $\mathbf{x}_{\bullet, k_\eta} > C_\eta$, respectively, depending on whether the k_η -th coordinate is greater than the splitting value C_η . With respect to every node $\eta \in \mathcal{T}$ in a tree structure, we adopt the notation $i \in \eta$ to indicate that the i -th sample (\mathbf{x}_i, y_i) or (\mathbf{z}_i, y_i) is assigned to the node η .

The recursive partition induced by a tree method is dictated by interpretable decision rules including the choice of splitting coordinates k_η and splitting values C_η . For any internal node η , let n_η be its size (i.e., the number of samples that fall into this node) and $\{y_i : 1 \leq i \leq n_\eta\}$ be the responses contained in η . CART selects (C_η, k_η) by

$$(C_\eta, k_\eta) = \arg \min_{C, k} \sum_{i \in \eta} (y_i - \mu_L^{C, k})^2 \mathbf{1}(\mathbf{x}_{i, k} \leq C) + \sum_{i \in \eta} (y_i - \mu_R^{C, k})^2 \mathbf{1}(\mathbf{x}_{i, k} > C), \quad (5)$$

where $(\mu_L^{C, k}, \mu_R^{C, k})$ are the sample average of responses within the left and right nodes that minimizes in-node sum of squares, i.e.,

$$\mu_L^{C, k} := \frac{\sum_{i \in \eta} y_i \cdot \mathbf{1}(\mathbf{x}_{i, k} \leq C)}{\sum_{i \in \eta} \mathbf{1}(\mathbf{x}_{i, k} \leq C)}, \quad \mu_R^{C, k} := \frac{\sum_{i \in \eta} y_i \cdot \mathbf{1}(\mathbf{x}_{i, k} > C)}{\sum_{i \in \eta} \mathbf{1}(\mathbf{x}_{i, k} > C)}. \quad (6)$$

Cycling through all internal nodes induces a recursive partition defined by the leaf nodes. In the existing tree literature (Quinlan, 1986; Breiman et al., 1987; Hastie et al., 2009), this partition is viewed as one of the predictor space, which indeed defines basis functions. These basis functions are used to approximate the regression function f in (1).

We take a slightly different perspective to view this partition as one that is induced by the observed samples, noting that the splitting action separates all observations $\mathcal{D}^{(N)}$ into two groups corresponding to the left and right children nodes.

Conceptually, the basis function view is at the population level operated on the support of f , while our analysis is inherently finite-sample and it operated on the indices of observations $[N] = \{1, \dots, N\}$. In particular, each internal node η collects a subset of observations and can be characterized by a subset of $[N]$, i.e., $\eta \subset [N]$, and the left and right child nodes of η lead to a finer partition of η by $\{i : \mathbf{x}_{i, k_\eta} \leq C_\eta, i \in \eta \subset [N]\}$, and $\{i : \mathbf{x}_{i, k_\eta} > C_\eta, i \in \eta \subset [N]\}$. As such, the recursive partition of the prediction space, once realized by finite samples, leads to a recursive

partition of $[N]$, which subsequently yields a recursive partition of $\mathcal{X}^{(N)}$ and $\mathcal{Y}^{(N)}$. As we shall show later, this finite-sample perspective connects tree methods with the ranking of $\mathcal{Y}^{(N)}$.

In the symbolic regression setting, a tree method sees the transformed features $\mathcal{Z}^{(N)}$ and $\mathcal{Y}^{(N)}$, and would proceed using the transformed symbolic features $\mathcal{Z}^{(N)}$ instead of $\mathcal{X}^{(N)}$ as predictor. We reiterate that these transformed features are of rapidly growing dimensionality and present high correlations, which require feature (pre-)selection as a necessary step in symbolic regression. Then fitting a regression tree using the transformed symbolic features, the criteria (6) contains a split along the feature space $\mathcal{Z}^{(N)}$:

$$\mu_L^{C,k} = \frac{\sum_{i \in \eta} y_i \cdot \mathbf{1}(z_{i,k} \leq C)}{\sum_{i \in \eta} \mathbf{1}(z_{i,k} \leq C)} = \frac{\sum_{i \in \eta} y_i \cdot \mathbf{1}(\theta_k \mathbf{x}_i \leq C)}{\sum_{i \in \eta} \mathbf{1}(\theta_k \mathbf{x}_i \leq C)}, \quad (7)$$

$$\mu_R^{C,k} = \frac{\sum_{i \in \eta} y_i \cdot \mathbf{1}(z_{i,k} > C)}{\sum_{i \in \eta} \mathbf{1}(z_{i,k} > C)} = \frac{\sum_{i \in \eta} y_i \cdot \mathbf{1}(\theta_k \mathbf{x}_i > C)}{\sum_{i \in \eta} \mathbf{1}(\theta_k \mathbf{x}_i > C)}. \quad (8)$$

Here, we omit the subscript and it is clear that $C = C_\eta$ associated with the node η . The first key observation from (7) and (8) is that by definition (2) the k -th coordinate of \mathbf{z}_i is obtained by applying the feature mapping θ_k to \mathbf{x}_i . Therefore, the split along the feature space $\mathcal{Z}^{(N)}$ can be attained by splitting along the original space $\mathcal{X}^{(N)}$. For example, if $\theta_k = \pi_1$, which projects onto the first coordinate, then splitting on the k -th coordinate of \mathbf{z}_i can be equivalently obtained from splitting along $\mathbf{x}_{i,1}$. The second key observation is that regardless of the growing dimensionality of q , the estimators (7) and (8) only rely on one splitting coordinate, making it particularly suitable for the symbolic regression scenario where q grows rapidly, as shown in Example 1.

In the rest of this paper, we focus on this feature set $\mathcal{Z}^{(N)}$, which includes the original data $\mathcal{X}^{(N)}$ as a special case where the transformation sets map \mathbf{x}_i to each of its coordinates such that $\mathbf{z}_i = \mathbf{x}_i$.

2.3 Local splits and principal decision ratio

In the sequel, we first analyze each internal node η and suppose η contains n_η observations indexed by $\{i(\eta) : i = 1, \dots, n_\eta\}$ using the original serial indices. For simplicity, we drop the dependence on η in the node-specific notation with the understanding that our analysis is generally applicable to any internal node η . For example, we will use (n, C, k) for (n_η, C_η, k_η) , respectively, and with a slight abuse of notation, use $[n] = \{1, \dots, n\}$ to denote the indices of the enclosed observations $\{i(\eta) : i = 1, \dots, n_\eta\}$.

At the stage of deciding the split (consisting of the splitting coordinate and splitting value), for any two pairs of decision rules (k_1, C_1) and (k_2, C_2) , we introduce the *principal decision ratio*:

$$\tau = \frac{\exp\left(-\sum_{i=1}^n (y_i - \mu_L^1)^2 \mathbf{1}(z_{i,k_1} \leq C_1) - \sum_{i=1}^n (y_i - \mu_R^1)^2 \mathbf{1}(z_{i,k_1} > C_1)\right)}{\exp\left(-\sum_{i=1}^n (y_i - \mu_L^2)^2 \mathbf{1}(z_{i,k_2} \leq C_2) - \sum_{i=1}^n (y_i - \mu_R^2)^2 \mathbf{1}(z_{i,k_2} > C_2)\right)}, \quad (9)$$

where $\mu_L^1 = \mu_L^{C_1, k_1}$ (and $\mu_R^1 = \mu_R^{C_1, k_1}$), $\mu_L^2 = \mu_L^{C_2, k_2}$ (and $\mu_R^2 = \mu_R^{C_2, k_2}$) as specified in (6). This means that we select splitting values from one of the observed input features \mathbf{z}_i 's, following the common practice in Breiman et al. (1987).

The numerator and denominator of (9) exponentiate the loss in Equation (5); this formulation assumes a Gaussian likelihood with unit error standard deviation, which is commonly used in model-based tree methods such as Bayesian CART (Chipman et al., 1998, 2002). Consequently, τ may represent a likelihood ratio. Based on τ , the splitting coordinate k and splitting value C that minimize the loss function (5) would have the highest τ value compared to any other splitting rules.

The principal decision ratio in (9) also encodes key information for Bayesian trees to make splitting decisions. In particular, the fitting procedure of Bayesian trees typically relies on an adapted form of τ . For Bayesian CART (Chipman et al., 1998) and its extension to sum-of-tree counterpart BART (Chipman et al., 2010), trees are sampled using a stochastic search via Markov chain Monte-Carlo that utilizes a Metropolis-Hastings ratio between the original tree and a proposed tree. And this ratio reduces to τ when comparing two splitting decisions. Similarly, Bayesian dyadic trees (Li and Ma, 2021) would draw posterior samples of partitioning directions with probabilities determined by all pairs of τ when the splitting values are restricted to halves of each coordinate. The exact posterior sampling procedures in these Bayesian tree methods also include inference on other parameters, such as the mean and standard deviation parameters at leaf nodes, and rules to prune a complete tree; for stochastic search, the Metropolis-Hastings ratio also involves other operations in addition to growing a tree via splitting internal nodes, such as the swapping operation.

Central to our analysis of tree methods is the principal decision ratio τ , and its interplay with ranking and feature selection. As explained, the principal decision ratio (9) is closely related to the loss function and Metropolis-Hastings ratio in a per-node strategy, which is advocated by Andronescu and Brodie (2009). Also analyzing a per-node strategy, Luo and Daniels (2021) observed that splits using relevant predictors yield higher Metropolis-Hastings ratios, indicating a preference for these predictors in the splitting process. This occurrence of τ , which we aim to substantiate with our analysis, exemplifies the intricate connection between feature selection and splitting decisions. Therefore, analyzing τ provides insight into how tree-based methods behave at local splits, and these per-node analyses findings will later be extended to the entire decision tree and tree ensembles.

3 Local Ranking at Local Splits

In this section, we will establish the connection between the response rankings (i.e., rankings of $\mathcal{Y}^{(N)}$) and the optimal principal decision ratios in a single tree. This leads to two observations which we summarize here at a high level:

1. The optimal partition of samples into children nodes depends only on the rankings of y , which we called the *oracle partition*. This oracle partition is solely determined by the ranks (or orders) of response y , in the sequential minimizations of the L_2 loss function (5) in splitting parameters C, k (where C can only be selected from samples), when the sizes of the nodes of the children are fixed. When children node sizes are not fixed, the minimization of L_2 loss involves the relative magnitude of the responses y .
2. However, the partitions in tree-based methods are determined by the actual configuration of predictors \mathbf{z} 's. This means that even if the oracle partition is completely determined by the responses y , we may only attain sub-optimal partitions in the form of $\{(\mathbf{z}_i, y_i) \mid \mathbf{z}_{i,k} \leq C\}$ and $\{(\mathbf{z}_i, y_i) \mid \mathbf{z}_{i,k} > C\}$ for some k and C .

We rewrite the loss function in (5) in a more general form as a function of partitions P_1, P_2

$$\mathcal{L}(P_1, P_2) = SS(P_1) + SS(P_2) =: \sum_{i:y_i \in P_1} (y_i - \mu_1^*)^2 + \sum_{i:y_i \in P_2} (y_i - \mu_2^*)^2, \quad (10)$$

where (P_1, P_2) is a 2-partition of $\{y_1, \dots, y_n\}$, and the internal sum of squares $SS(P) := \sum_{i:y_i \in P} (y_i - \mu(P))^2$ with $\mu(P) = \frac{1}{|P|} \sum_{i:y_i \in P} y_i$. Then the loss function in (5) is $\mathcal{L}(P_1, P_2)$ when (P_1, P_2) are constrained to take the form $P_1 = \{y_i : \mathbf{z}_{i,k} \leq C\}$ and $P_2 = \{y_i : \mathbf{z}_{i,k} > C\}$, and μ_1^*, μ_2^* are the corresponding means of y_i 's associated with these two partitions. This function $\mathcal{L}(P_1, P_2)$ is invariant to the ordering of (P_1, P_2) , and its optimal solution is expected to be unique only up to this ordering.

3.1 Optimal 2-partition

We next study the optimal partition without imposing the aforementioned predictor-dependent constraints on the partition induced by a tree method. This study is applicable to any selected coordinate $k \in [q]$. We begin with an illustrative example that contains 5 observations where we assume the dimensionality q of $\mathcal{Z}^{(N)}$ to be 1 for the ease of visualization in Figure 2 but the argument works regardless of q .

Example 2 (*5-sample example oracle 2-partition with fixed partition sizes*) Assume $n = 5$ and consider 2-partitions (P_1, P_2) with sizes $(2, 3)$. We proceed with the explicit computation of the loss function (10). First consider the 2-partition with $P_1 = \{y_{(1)}, y_{(3)}\}$ and $P_2 = \{y_{(2)}, y_{(4)}, y_{(5)}\}$:

$$SS(P_1) = \left(y_{(1)} - \frac{y_{(1)} + y_{(3)}}{2} \right)^2 + \left(y_{(3)} - \frac{y_{(1)} + y_{(3)}}{2} \right)^2 = \frac{1}{2} (y_{(1)} - y_{(3)})^2,$$

$$\begin{aligned} SS(P_2) &= \left(y_{(2)} - \frac{y_{(2)} + y_{(4)} + y_{(5)}}{3} \right)^2 + \left(y_{(4)} - \frac{y_{(2)} + y_{(4)} + y_{(5)}}{3} \right)^2 + \left(y_{(5)} - \frac{y_{(2)} + y_{(4)} + y_{(5)}}{3} \right)^2 \\ &= \left(\frac{2y_{(2)} - y_{(4)} - y_{(5)}}{3} \right)^2 + \left(\frac{-y_{(2)} + 2y_{(4)} - y_{(5)}}{3} \right)^2 + \left(\frac{-y_{(2)} - y_{(4)} + 2y_{(5)}}{3} \right)^2 \\ &= \frac{1}{9} \left(6y_{(2)}^2 + 6y_{(4)}^2 + 6y_{(5)}^2 - 6y_{(2)}y_{(4)} - 6y_{(4)}y_{(5)} - 6y_{(2)}y_{(5)} \right). \end{aligned}$$

Similarly, for the 2-partition with $P_1 = \{y_{(1)}, y_{(2)}\}$ and $P_2 = \{y_{(3)}, y_{(4)}, y_{(5)}\}$, we have

$$SS(P_1) = \frac{1}{2} (y_{(1)} - y_{(2)})^2, \quad SS(P_2) = \frac{1}{9} \left(6y_{(3)}^2 + 6y_{(4)}^2 + 6y_{(5)}^2 - 6y_{(3)}y_{(4)} - 6y_{(4)}y_{(5)} - 6y_{(3)}y_{(5)} \right).$$

Taking the difference of these two sets of expressions (note that $y_{(1)} < y_{(2)} < y_{(3)} < y_{(4)} < y_{(5)}$) shows that the change of $SS(P_1)$ and $SS(P_2)$, respectively denoted by Δ_1 and Δ_2 , are both greater than zero:

$$\begin{aligned} \Delta_1 &= \frac{1}{2} (y_{(1)} - y_{(3)})^2 - \frac{1}{2} (y_{(1)} - y_{(2)})^2 = \frac{1}{2} (y_{(2)} - y_{(3)}) (y_{(1)} - y_{(3)} + y_{(1)} - y_{(2)}) > 0, \\ \Delta_2 &= \frac{1}{9} \left(6y_{(2)}^2 + 6y_{(4)}^2 + 6y_{(5)}^2 - 6y_{(2)}y_{(4)} - 6y_{(4)}y_{(5)} - 6y_{(2)}y_{(5)} \right) \\ &\quad - \frac{1}{9} \left(6y_{(3)}^2 + 6y_{(4)}^2 + 6y_{(5)}^2 - 6y_{(3)}y_{(4)} - 6y_{(4)}y_{(5)} - 6y_{(3)}y_{(5)} \right) \\ &= \frac{1}{9} \left(6y_{(2)}^2 - 6y_{(3)}^2 - 6(y_{(2)} - y_{(3)})y_{(4)} - 6(y_{(2)} - y_{(3)})y_{(5)} \right) \\ &= \frac{2}{3} (y_{(2)} - y_{(3)}) (y_{(2)} + y_{(3)} - y_{(4)} - y_{(5)}) > 0. \end{aligned}$$

Therefore, the second 2-partition exchanging $y_{(2)}$ and $y_{(3)}$ reduces the total sum $\mathcal{L}(P_1, P_2)$ in (10). Using this argument repeatedly, we will arrive at the conclusion that $P_1 = \{y_{(1)}, y_{(2)}\}$ and $P_2 = \{y_{(3)}, y_{(4)}, y_{(5)}\}$ form a (locally) optimal 2-partition with sizes $(2, 3)$. Similarly, another (local) optimal 2-partition with sizes $(2, 3)$ is $P_1 = \{y_{(4)}, y_{(5)}\}$ and $P_2 = \{y_{(1)}, y_{(2)}, y_{(3)}\}$. From their expressions, we can see that only the ranks and the magnitude of the difference between responses affect the Δ_1 and Δ_2 .

Like expressions (7) and (8), the oracle partition depends only on the response values y 's. The second column in Figure 2 shows two possible configurations based on the two datasets shown in

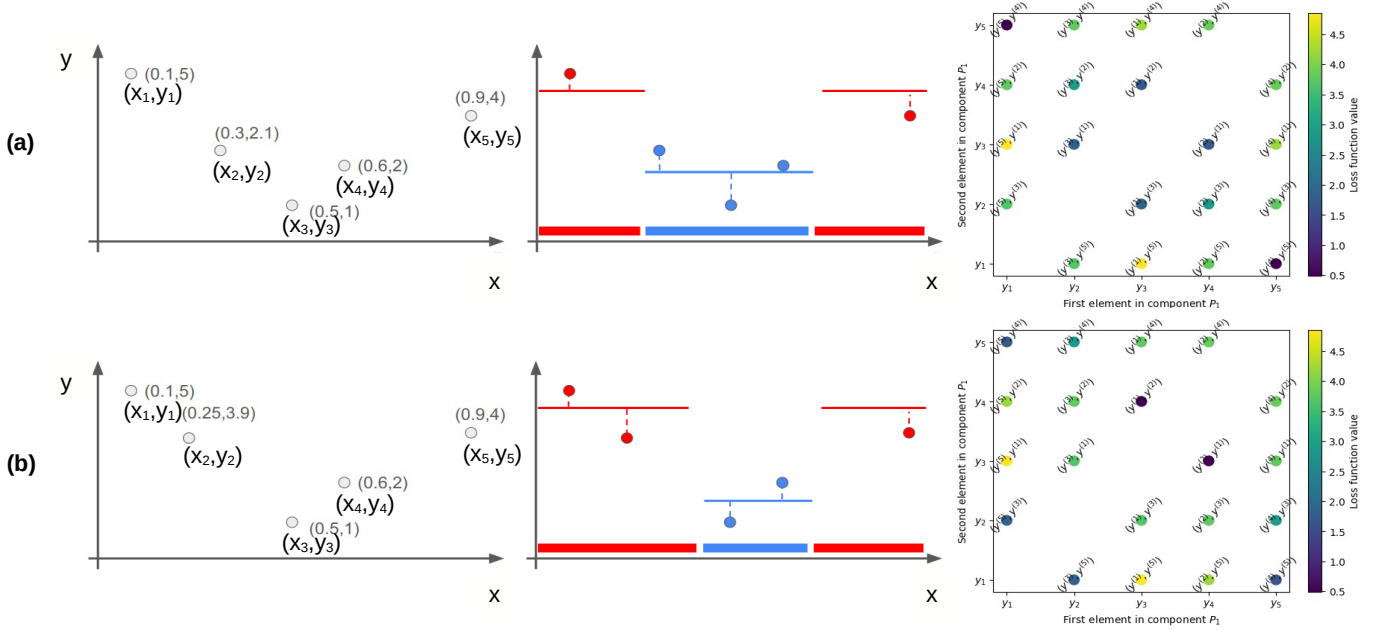


Figure 2: A depth 2 tree with 5 observations showing two possible oracle partitions in Lemma 1. In the first column, we present the raw (x_i, y_i) pair of dataset; In the second column, we present the oracle partition using red and blue colors, and the support of indicator functions on the x -axis. The horizontal solid lines represent the group mean of y values (as prediction value as well); the vertical dashed lines represent the point-to-mean distances. In the third column, we illustrate the loss function (10) The minimum in row (a) is attained by $\{y_{(4)}, y_{(5)}\} = \{y_1, y_5\}$ and $\{y_{(1)}, y_{(2)}, y_{(3)}\} = \{y_2, y_3, y_4\}$. The minimum in row (b) is attained by $\{y_{(3)}, y_{(4)}, y_{(5)}\} = \{y_1, y_2, y_5\}$ and $\{y_{(1)}, y_{(2)}\} = \{y_3, y_4\}$. We color the dots by the actual loss function values, and annotate the ordered statistics near each dot.

the first column of the same figure. In both rows (a) and (b), the x -axis is the first element in the size 2 partition component P_1 , y -axis is the second element in size 2 partition component P_1 , therefore the figure is symmetric. The minimum is attained by $P_1^* = \{y_{(1)}, y_{(2)}\} = \{y_3, y_4\}$ and $P_2^* = \{y_{(3)}, y_{(4)}, y_{(5)}\} = \{y_1, y_2, y_5\}$, or $P_1^{**} = \{y_{(4)}, y_{(5)}\} = \{y_2, y_5\}$ and $P_2^{**} = \{y_{(1)}, y_{(2)}, y_{(3)}\} = \{y_3, y_4, y_1\}$.

Example 2 serves as a representative case for our result applicable to general sample sizes, as formalized in the lemma below.

Lemma 1 (Oracle 2-partition with fixed sizes) For a 2-partition of n elements $y_{(1)} < y_{(2)} < \dots < y_{(n)}$ into components of size i and $n - i$, we assume that $n > 4$, $\min(n - i, i) \geq 2$ to ensure variances are defined. Then the following partitions

- $P_1^* = \{y_{(1)}, y_{(2)}, \dots, y_{(i)}\}$ and $P_2^* = \{y_{(i+1)}, y_{(i+2)}, \dots, y_{(n)}\}$ OR,
- $P_1^{**} = \{y_{(1)}, y_{(2)}, \dots, y_{(n-i)}\}$ and $P_2^{**} = \{y_{(n-i+1)}, y_{(i+2)}, \dots, y_{(n)}\}$

are the only 2-partitions of size i and $n - i$ that minimize (10).

Proof See Appendix A. ■

Remark 2 *The lemma 1 states that the loss function only has two local minima attained by (P_1^*, P_2^*) (corresponding to size $(i, n-i)$) or (P_1^{**}, P_2^{**}) . Comparing the loss function value (10) at (P_1^*, P_2^*) or (P_1^{**}, P_2^{**}) gives the global minimum of the loss function, hence determining the split maximizing (9). This optimal 2-partition, however, may not be attained by those 2-partitions induced by splitting on z values only once. Lemma 1 is a refined version of optimal splits in trees with continuous outcome under L^2 loss, which was studied as a grouping problem instead of a ranking problem in Fisher (1958).*

We next present a simple example to demonstrate Lemma 1 and the induced partitions on the response and input coordinates.

Example 3 *(5-sample oracle 2-partition with varying partition sizes) Now we consider the same dataset as in Example 2 but we do not fix the partition sizes to $(2, 3)$ any more.*

In the third column of Figure 2, we show the oracle 2-partitions on the response y and the corresponding landscape of the loss function (10). In panel (a), we put $(x_1, y_1) = (0.1, 5)$, $(x_2, y_2) = (0.3, 2.1)$, $(x_3, y_3) = (0.5, 1)$, $(x_4, y_4) = (0.6, 2)$, $(x_5, y_5) = (0.9, 4)$, and the oracle partition that minimizes the total sum is $\{y_{(1)}, y_{(2)}, y_{(3)}\}$ of size 3 and $\{y_{(4)}, y_{(5)}\}$ of size 2. In panel (b), we put $(x_2, y_2) = (0.25, 3.9)$, but the rest of the pairs remain the same, and the oracle partition that minimizes the total sum is $\{y_{(1)}, y_{(2)}\}$ of size 2 and $\{y_{(3)}, y_{(4)}, y_{(5)}\}$ of size 3. It turns out that the oracle 2-partition of size $(2, 3)$ is indeed the configuration that minimizes the (10), compared to oracle 2-partitions of size $(1, 4)$.

Note that if we observe $(z_1, y_1), \dots, (z_5, y_5)$ instead: since the oracle partition for the loss function depends only on the response y 's, this does not affect our oracle partition above. However, it is clear from Figure 2 that each of the two candidate optimal partitions (in the sense that they minimize (10)) P_1^*, P_2^* or P_1^{**}, P_2^{**} creates 3 partition components on the \mathcal{X} domain, which cannot be attained by splitting on x values only once. If we choose the transformed symbolic feature $z = x^2$, then the oracle 2-partition for y can be realized by partitioning on \mathcal{Z} domain.

Remark 3 *Applying Lemma 1 repeatedly leads to solutions to finding optimal 2-partitions with varying sizes. In particular, for $y_{(1)} < y_{(2)} < \dots < y_{(n)}$ with $n > 4$, the loss function (10) is minimized by solving the following problem:*

$$\min_{i \in \{1, 2, \dots, n-1\}} \sum_{j=1}^i (y_{(j)} - \mu_1^*)^2 + \sum_{j=i+1}^n (y_{(j)} - \mu_2^*)^2 = \min_{i \in \{1, 2, \dots, n\}} \mathcal{L}(P_1, P_2), \quad (11)$$

and form the associated partitions. There are still two possible minimizers for (11) as stated in Lemma 1. From the angle of grouping (Fisher, 1958) or analysis of variance (ANOVA), the problem of (11) can be considered as finding a division of \mathcal{Y} into two groups such that the in-group variance is as small as possible. In other words, the resulting minimizer would produce “most in-group homogeneous” group partitions. The optimal 2-partition for components with varying sizes depends not only on the ranking information, as it would for the oracle 2-partition with fixed sizes, but also on the distribution information of the responses y .

However, most tree models create partitions on x 's (e.g., which is a special case with $q = 1, z \in \mathbb{R}$) but not y 's domain for prediction purposes, so how well we can predict depends on how “similar” (or “concordant”) the response rankings and input rankings are. For example, if the inputs x 's and the responses y 's have the same rankings, then the oracle 2-partition on response can be realized

by corresponding oracle 2-partition on x 's. The following corollary 4, which is straightforward from Lemma 1, gives a sufficient and necessary condition to attain oracle 2-partitions when splitting only on x .

Corollary 4 (*Oracle 2-partition with fixed sizes with univariate x*) For a 2-partition of n elements $y_{(1)} < y_{(2)} < \dots < y_{(n)}$ into components of fixed size i and $n-i$, we assume that $n > 4$, $\min(n-i, i) > 2$ and assume that there exists some C such that

- $P_1^* = \{y_{(1)} < y_{(2)} < \dots < y_{(i)}\} = \{y' \mid \text{the pair } (x, y) \text{ s.t. } x \leq C\}$, and $P_2^* = \{y_{(i+1)} < y_{(i+2)} < \dots < y_{(n)}\} = \{y' \mid \text{the pair } (x, y) \text{ s.t. } x > C\}$.
- $P_1^{**} = \{y_{(1)} < y_{(2)} < \dots < y_{(n-i)}\} = \{y' \mid \text{the pair } (x, y) \text{ s.t. } x \leq C\}$, and $P_2^{**} = \{y_{(n-i+1)} < y_{(n-i+2)} < \dots < y_{(n)}\} = \{y' \mid \text{the pair } (x, y) \text{ s.t. } x > C\}$.

Then these are the only 2-partitions of size i and $n-i$ that minimize (10).

This means that a sufficient condition for us to attain optimal partition by splitting once on x is that the ranks of x and y are the same or linearly related. In fact, when the input and response rankings are the same, the CART loss function described by Scornet et al. (2015) formula (2) or Hastie et al. (2009) Chapter 9, takes the following form. When input and response rankings are the same and $x_{(i)} \leq C < x_{(i+1)}$ the following loss function value remains the same:

$$\min_{i \in \{1, 2, \dots, n\}} \left(\sum_{j=1}^i (y_{(j)} - \mu_1^*)^2 + \sum_{j=i+1}^n (y_{(j)} - \mu_2^*)^2 \right) = (10) = (11).$$

In this case, such x with the same ranking of y will be the most likely splitting coordinate. We next provide two such examples using monotonic transformation and interpolators, respectively.

Example 4 (*Monotonic transformation*) Suppose that $d = 1$ and noiseless $y(x) = f(x)$ is a monotonic function of univariate $x \in \mathbb{R}$, then choosing any observation $x \in \mathcal{X}^{(N)}$ as a splitting value will give us an oracle 2-partition corresponding to the fixed sizes. This is because under monotonic transformation $\theta = f$, splitting on any observed x is equivalent to an oracle 2-partition on y . By Lemma 1, there cannot be any other 2-partition of the same size on y that gives us a strictly larger principal decision ratio.

Furthermore, if we assume that $z = \theta_1 x$ for $d = 1$ and another θ_1 that is monotonic as well, then we can come to the expected conclusion that $y(x) = f(\theta_1 x)$ always induces the optimal 2-partition, since $\theta \circ \theta_1 = f \circ \theta_1$ is again monotonic. This example shows that when the true underlying function is monotonic, it will induce an oracle partition on \mathcal{X} and \mathcal{Y} domains simultaneously.

Example 5 (*Interpolator*) Suppose that $d = 1$, then for any pairs of (x_i, y_i) for $i = 1, \dots, n$, we can construct an n -degree polynomial interpolator, denoted by g as a mapping, such that $y_i = g(x_i)$ for all i . This transformed symbolic feature $z = g(x)$ maintains the same ranking of the response and thus attains the optimal oracle 2-partition. Then, by Corollary 4, using the output of such an interpolator as input will always maximize the (10) and hence the principal decision ratio. Even without exact interpolation, when $n \ll q$, it is easy to observe over-fitting, which means we can use the transformed features to construct such an interpolator mapping. This example shows a major difference between finite-sample and asymptotic scenarios.

Therefore, a decision tree tends to split on a feature for which the response is a monotonic transformation, and likewise, an interpolator would be the most likely splitting feature if seen by

the tree. This perfectly explains the fact that decision tree is scale-invariant in the sense that its prediction remains unchanged if we multiply the input by a scalar as noted in Bleich et al. (2014). In fact, this shows a stronger result that it is multi-way scale-invariant. Namely, if we simply multiply possibly different but non-zero scalars to each coordinate of input features, the principal decision ratio still remains unchanged (since multiplying a non-zero scalar is a monotonic transformation and preserves the ranks). While the inability of decision trees to distinguish between monotonic transformations is well known in the literature (Bleich et al., 2014), interpolators are less discussed but an interesting example that shows there always exists a mapping in finite sample sizes to mislead decision trees. Such data-dependent mappings are typically ruled out in the pool of symbolic expressions considered in symbolic selection, making it more robust to regular regressions.

We next analyze the principal decision ratios when selecting between a more general class of transforms that generates symbolic features \mathbf{z} from \mathbf{x} , other than the two examples above.

3.2 Piece-wise monotonic transforms

We now analyze the splitting behavior of the decision trees when selecting features \mathbf{z} generated by transformations. Such selection is crucial in symbolic regressions (See Example 1). In particular, we consider piece-wise monotonic transforms, which are widely used to generate symbolic features and are also of interest due to their flexibility, as they can approximate well a sufficiently large class of transformations of interest (Newman et al., 1972).

Throughout this section, we consider two generic features $\mathbf{z}_{i,k_1} = \theta_1 \mathbf{x}_i$ and $\mathbf{z}_{i,k_2} = \theta_2 \mathbf{x}_i$ for an arbitrary i (in shorthand, $\mathbf{z}_k = \theta \mathbf{x}_k$), where both θ_1 and θ_2 are piece-wise monotonic in the form of $\theta \mathbf{x}_{i,k}$, where univariate mappings θ transforms the k -th coordinate of \mathbf{x} .

A piece-wise monotonic transform θ defined on \mathbb{R} is characterized by a partition, which consists of finitely many disjoint intervals (i.e., monotonic intervals) on each θ is monotonic. Such partitions are not unique as one can always divide a subset while maintaining the strict monotonicity of θ on the finer partition. Unless stated otherwise, we always choose the partition with the smallest cardinality.

We aim to characterize the principal decision ratio at two pairs of splitting values and coordinates (C_1, k_1) and (C_2, k_2) , i.e., the ratio of

$$\sum_{i=1}^n \left(y_i - \mu_L^{C_1, k_1} \right)^2 \mathbf{1}(\mathbf{z}_{i, k_1} \leq C_1) + \sum_{i=1}^n \left(y_i - \mu_R^{C_1, k_1} \right)^2 \mathbf{1}(\mathbf{z}_{i, k_1} > C_1) \quad (12)$$

and

$$\sum_{i=1}^n \left(y_i - \mu_L^{C_2, k_2} \right)^2 \mathbf{1}(\mathbf{z}_{i, k_2} \leq C_2) + \sum_{i=1}^n \left(y_i - \mu_R^{C_2, k_2} \right)^2 \mathbf{1}(\mathbf{z}_{i, k_2} > C_2). \quad (13)$$

The following definitions and simple properties of θ_1 and θ_2 are useful.

Definition 5 (*Refined monotonic intervals*) Consider two piece-wise monotonic transforms θ_1 and θ_2 mapping from \mathbb{R} onto \mathbb{R} , with monotonic intervals \mathcal{I}_1 and \mathcal{I}_2 on \mathbb{R} respectively. We define the refined monotonic intervals for the transformation pair (θ_1, θ_2) to be the collection of intervals $\mathcal{I}_{1 \cap 2} := \{I = I_1 \cap I_2 \mid I_1 \in \mathcal{I}_1, I_2 \in \mathcal{I}_2\}$.

The refined monotonic intervals $\mathcal{I}_{1 \cap 2}$ is a new partition of the x -domain induced by (θ_1, θ_2) . On each refined monotonic interval $I \in \mathcal{I}_{1 \cap 2}$, the two piece-wise monotonic transforms θ_1 and θ_2 are both monotonic; that is, the restricted transforms $\theta_1|_I$ and $\theta_2|_I$ are both monotonic. The next result follows directly from Definition 5 but introduces pre-images of the restricted transforms that are useful to study the principal decision ratio.

Corollary 6 *On each refined monotonic interval $I \in \mathcal{I}_{1 \cap 2}$ and for any value $C \in \mathbb{R}$, the piece-wise monotonic transform θ_1 and θ_2 can have 0 or 1 pre-image. That means, there exists 0 or 1 value $t \in I$ such that the restricted transform $\theta_1|_I(t) = C$ and $\theta_2|_I(t) = C$.*

We next study the principal decision ratio of these two transformations at arbitrary splitting values C_1 and C_2 . Although θ_1 and θ_2 are not necessarily globally invertible, they are invertible on each refined monotonic interval $I \in \mathcal{I}_{1 \cap 2}$. By definition (2), we note that $\mathbf{z}_{i,k_1} \leq C_1$ can be written as $\theta_1 \mathbf{x}_{i,k} \leq C_1$, which can be reduced to $\mathbf{x}_{i,k} \leq \theta_1^{-1} C_1$ on each $I \in \mathcal{I}_{1 \cap 2}$ where $\theta_1^{-1} C_1$ is well-defined. Using Corollary 6, for a refined interval $I \in \mathcal{I}_{1 \cap 2}$ we can link the relative magnitude of principal decision ratio τ to the behavior of covariate \mathbf{x} instead of \mathbf{z} . The following result Proposition 7 is consistent with the discussion that splitting will decrease the Bayes risk in Section 9.3 and Theorem 9.5 of Breiman et al. (1987).

Proposition 7 *For any splitting value $C \in \mathbb{R}$, the means $\mu_L^{C,k}, \mu_R^{C,k}$ defined for \mathbf{z} as in (8), the parent node mean μ^\sharp , and the k -th coordinate \mathbf{z}_k , we have*

$$\begin{aligned} & \sum_{i=1}^n (y_i - \mu_L^{C,k})^2 \mathbf{1}(\mathbf{z}_{i,k} \leq C) + \sum_{i=1}^n (y_i - \mu_R^{C,k})^2 \mathbf{1}(\mathbf{z}_{i,k} > C) = \\ & \sum_{i=1}^n (y_{(i)} - \mu_L^{C,k})^2 \mathbf{1}(\mathbf{z}_{(i),k} \leq C) + \sum_{i=1}^n (y_{(i)} - \mu_R^{C,k})^2 \mathbf{1}(\mathbf{z}_{(i),k} > C) \leq \sum_{i=1}^n (y_{(i)} - \mu^\sharp)^2, \end{aligned}$$

where the equality holds if and only if $\mu_L^{C,k} = \mu_R^{C,k} = \mu^\sharp$.

Proof See Appendix B. ■

In the spirit of Theorem 9.5 of Breiman et al. (1987), we can see from the above argument that a feature mapping that induces more splits will be favored in the sense that it increases the principal decision ratio, hence the likelihood for the splitted children nodes. This helps compare two transformations in terms of the existence of pre-images, or to “contrast” these two transformations at a finer resolution level. Below, we start with an illustrative example, followed by its generalization.

Example 6 *Let us consider the following three cases with fixed $\theta_1(x) = x + 1.2$, $\theta_2(x) = -4x^2 + 4x$, with $\mathcal{I}_1 = \{[0, 1]\}$, $\mathcal{I}_2 = \{[0, 1/2], [1/2, 1]\}$, and the refined monotonic intervals $\mathcal{I}_{1 \cap 2} = \{[0, 1/2], [1/2, 1]\}$. And we consider expressions in (12), (13) along with $\mathbf{z}_{i,k_1} = \theta_1 \mathbf{x}_i$ and $\mathbf{z}_{i,k_2} = \theta_2 \mathbf{x}_i$, as illustrated by Figure 3. We can consider the following cases:*

Let us consider $I = [0, 1/2]$ first, if we fixed $C_1 \in (-\infty, 1.2) \cup (2.2, \infty)$ and choose $C_2 \in (-\infty, 0) \cup (1, \infty)$ as shown in the (a) in Figure 3. We cannot differentiate between θ_1 and θ_2 based solely on the principal decision ratio when splitting on inputs $\mathbf{x} \in I$, since both θ_1 and θ_2 will have 0 pre-image in I , so the corresponding splits associated with C_1, C_2 have the same chance of being selected on this interval. However, if we choose $C_1 \in (1.2, 1.7)$ or $[1.7, 2.2)$, $C_2 \in (-\infty, 0) \cup (1, \infty)$ in such a way shown as (b) or (c), then over the $I = [0, 1/2]$ or $[1/2, 1]$ we have a higher chance of selecting θ_1 from analysis of expressions in (12), (13). If we fixed $C_1 \in (-\infty, 1.2) \cup (2.2, \infty)$, $C_2 \in [0, 1]$ this analysis remains the same and we learn that (d) in Figure 3 can differentiate θ_1, θ_2 .

Now if we choose $C_1 \in [1.2, 2.2]$, $C_2 \in [0, 1]$, then θ_1, θ_2 will both have 1 pre-image in I as shown in (e) and (f) in Figure 3. Then we are back to the computation of (11). The detailed analysis will be given in Example 7.

The observation in the above example can be summarized as the following result linking the principal decision ratios and the refined intervals of a given univariate feature mapping.

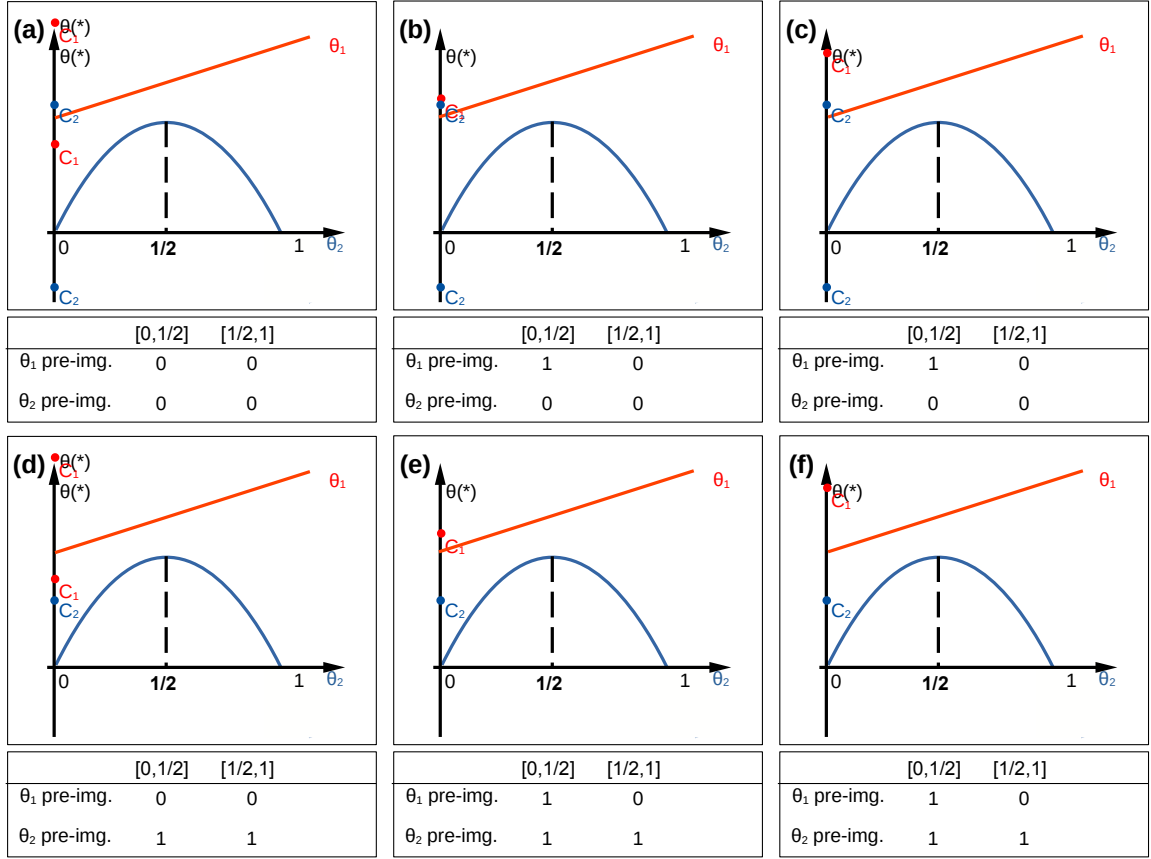


Figure 3: Refined monotonic intervals $\mathcal{I}_2 = \{[0, 1/2], [1/2, 1]\}$ for the $\theta_1(x) = x$, $\theta_2(x) = -4x^2 + 4x$ shown. We use vertical black dashed lines to illustrate the refined monotonic intervals, and count the number of pre-images for θ_1, θ_2 over each refined intervals.

Proposition 8 Consider one splitting variable \mathbf{x}_k for a fixed $k \in \{1, 2, \dots, d\}$ and two piecewise strictly monotonic transformations θ_1 and θ_2 with refined monotonic intervals $\mathcal{I}_{1 \cap 2}$. For any $C_1, C_2 \in \mathbb{R}$ and any $I \in \mathcal{I}_{1 \cap 2}$, we have

(i) When θ_1 and θ_2 have 0 pre-image for C_1 and C_2 on I , the principal decision ratio is 1 for the transformed variates $\theta_1 \mathbf{x}_k$ and $\theta_2 \mathbf{x}_k$ over this interval $I \in \mathcal{I}_{1 \cap 2}$.

(ii) When θ_1 and θ_2 have different numbers of pre-images for C_1 and C_2 on I , the principal decision ratio is larger for the transform with 1 pre-image over this interval $I \in \mathcal{I}_{1 \cap 2}$.

(iii) When θ_1 and θ_2 have 1 pre-image for C_1 and C_2 on I , the principal decision ratio is larger for the transform θ_i that solves the following problem:

$$\min_{j=1,2} \sum_{i=1}^n (y_i - \mu_L^j)^2 \mathbf{1}(\mathbf{x}_{i,k_j} \leq \theta_j^{-1} C_j) + \sum_{i=1}^n (y_i - \mu_R^j)^2 \mathbf{1}(\mathbf{x}_{i,k_j} > \theta_j^{-1} C_j)$$

When $k_1 = k_2 = k$ and $C_1 = C_2 = C$, this reduces to (11).

Proof See Appendix C. ■

Using the characterization in Proposition 8, the probability of θ_1 having a larger principal decision

ratio when compared to θ_2 can be calculated as follows. Let x be the k -th coordinate of \mathbf{x} , i.e., \mathbf{x}_k . In practice we usually use $C_1 = C_2 = C$, and it is not hard to exclude the case (iii) in the above Proposition 8: Example 4 tells us that $\theta_1 + C_0$ and θ_1 for $C_0 \in \mathbb{R}$ will not change principal decision ratio τ . Assuming that $\sup \theta_2$ and $\inf \theta_1$ are finite, we can pick $C_0 = \sup \theta_2 - \inf \theta_1 + 1$ to ensure that any $C_1 = C_2 = C$ will not lead to the case (iii).

Proposition 9 *Under the assumption of Proposition 8 and there is not I where both θ_1, θ_2 both have 1 pre-images, assume additionally that the input location \mathbf{x} is distributed as \mathbb{P} and denote the $N_1 + N_2$ refined monotonic intervals as*

- $I_1^1, \dots, I_1^{N_1}$ where θ_1 has 1 pre-image and θ_2 has 0 pre-image of C (θ_1 has higher chance of being selected);
- $I_2^1, \dots, I_2^{N_2}$ where θ_2 has 1 pre-image and θ_1 has 0 pre-image of C (θ_2 has higher chance of being selected).

Then, the probability that the principal decision ratio prefers θ_1 over θ_2 can be computed as

$$p_{1>2} = \sum_{i=1}^{N_1} \int_{I_1^i} 1d\mathbb{P} - \sum_{j=1}^{N_2} \int_{I_2^j} 1d\mathbb{P} = \mathbb{P} \left(\bigcup_{i=1}^{N_1} I_1^i \right) - \mathbb{P} \left(\bigcup_{j=1}^{N_2} I_2^j \right). \quad (14)$$

Note that these intervals $I_1^1, \dots, I_1^{N_1}$ and $I_2^1, \dots, I_2^{N_2}$ are dependent on the fixed transformation pair (θ_1, θ_2) and it is possible to optimize over C_1 and C_2 to maximize (or minimize) the quantity $p_{1>2}$ in (14).

Example 7 ($p_{1>2}$ calculation) *Suppose that \mathbb{P} is the uniform measure on $[0, 1]$, and consider $\theta_1(x) = x + 1.2$, $\theta_2(x) = -4x^2 + 4x$ with $C_1 = C_2 = C$ as in Example 6, and the refined monotonic intervals $\mathcal{I}_2 = \{[0, 1/2], [1/2, 1]\}$. Applying (14) leads to*

$C \in (-\infty, 0)$	$C \in (0, 1)$	$C \in [1, 1.2)$	$C \in [1.2, 1.7)$	$C \in [1.7, 2.2)$	$C \in (2.2, \infty)$
case (i)	$I_2^1 = [0, 1]$	case (i)	$I_1^1 = [0, 1/2]$	$I_1^2 = [1/2, 1]$	case (i)

For other C 's, if we assume \mathbb{P} is uniform, probabilities $p_{1>2}$ can be filled in as:

$C \in (-\infty, 0)$	$C \in (0, 1)$	$C \in [1, 1.2)$	$C \in [1.2, 1.7)$	$C \in [1.7, 2.2]$	$C \in (2.2, \infty)$
0.	1.	0.	0.5	0.5	0.

With this table, one can observe that the value of $p_{1>2}$ can be maximized by choosing $C \in [1.2, 2.2]$; and it can be minimized by choosing $C \in (0, 1)$.

4 Global Rankings with Regressions

The ranking perspective established in preceding sections is focused on local splits. We now turn to extending this perspective to study the global performance of tree-based methods, including both a single tree consisting of multiple splits and tree ensembles, in terms of ranking. In this section, we always consider the full dataset of size N instead of node-specific sample size n . On this full dataset, we will show that tree-based methods such as CART and BART, when trained in a supervised regression context, yield good ranking performance.

Throughout this section, we consider the model (1) as a “noisy scoring” model. In particular, the mean function f , now considered as a scoring function, takes the feature \mathbf{x}_i and assign it

a “score” $f(\mathbf{x}_i)$, and its noisy “score” is y_i . Any scoring function f can induce a permutation $r = \{j_1, j_2, \dots, j_N\}$ on the full set of $\{1, 2, \dots, N\}$ with the same cardinality, such that $f(\mathbf{x}_{j_1}) \geq f(\mathbf{x}_{j_2}) \geq \dots \geq f(\mathbf{x}_{j_N})$. We consider the following criterion to assess the ranking performance of scoring functions f through r :

$$\mathbf{T}(r) = \frac{2}{N(N-1)} \sum_{i=1}^{N-1} \sum_{i'=i+1}^N (\mathbb{E}_{y_{j_i}|\mathbf{x}_{j_i}} y_{j_i} - \mathbb{E}_{y_{j_{i'}}|\mathbf{x}_{j_{i'}}} y_{j_{i'}}), \quad (15)$$

which has been studied in the ranking literature such as Cossock and Zhang (2006) and can be also generalized to operate on subsets instead of the full dataset. Note that previously we considered rankings with actual responses y_i 's; in the presence of noise, the metric in (15) consider orderings on the *conditional means* instead of orderings on the responses y_j in (3) to avoid the noise effect.

The *Bayes-scoring function* $f_B(\mathbf{x}_j) = \mathbb{E}_{y_j|\mathbf{x}_j} y_j$ is defined as the conditional expectation of y_j conditioning on the j -th input \mathbf{x}_j . Its included permutation, denoted by r_B , maximizes $\mathbf{T}(r)$ in (15) (see, e.g., Cossock and Zhang (2006)). Hence, the Bayes rank can be defined by this permutation r_B that sorts the conditional means, and the (15) measures how any other permutation deviates from this “optimal permutation”. From this discussion, we can see that the optimal rank-preserving function is not unique and can be obtained from pre-composite monotonic transformations to f_B like $\tau \circ f_B$.

We are now in a position to establish oracle bounds under the ranking metric $\mathbf{T}(r)$ for a fully-split single CART tree with *finite samples*, based on the oracle properties from Klusowski and Tian (2024). Consider the function class \mathcal{G} that collects functions with an additive form $f(\mathbf{x}) = \sum_{i=1}^d f_i(\mathbf{x}_i)$, where each coordinate $f_i: \mathbb{R} \rightarrow \mathbb{R}$ has bounded variation (hence f has bounded variation), and the \mathcal{G}_0 is a pre-chosen model class that might deviate from \mathcal{G} as set up in Klusowski and Tian (2024), which allows for possible model misspecification. Here we need this pre-chosen model class \mathcal{G}_0 to contain \mathcal{G} . We consider a random design where $\mathcal{X}^{(N)}$ is a simple random sample of a distribution \mathbb{P}_X . For a function f , its ℓ_2 norm is defined as $\|f\|^2 = \int f(u)^2 d\mathbb{P}_X(u)$, and its supremum norm is denoted as $\|f\|_\infty$.

Theorem 10 (*Oracle inequality for ranking*) *Suppose that the Bayes scoring function $f_B \in \mathcal{G}_0 \subset \mathcal{G}$ and that we have a complete binary regression tree $g_{c,K}$ of depth $K \geq 1$ constructed by CART. Then the permutation $r_{c,K}$ induced by $g_{c,K}$ satisfies*

$$\begin{aligned} & \mathbb{P}_{(\mathcal{X}^{(N)}, \mathcal{Y}^{(N)})} (\mathbf{T}(r_B) - \mathbf{T}(r_{c,K}) > \varepsilon_N) \\ & \leq \frac{1024}{\varepsilon_N^4} \cdot \inf_{g \in \mathcal{G}} \left\{ \|f_B - g\|^2 + \frac{\|g\|_{TV}^2}{K+3} + C_B \frac{2^K \log^2 N \log(Nd)}{N} \right\} + \frac{32R_\infty J_0(2R_2, \mathcal{G}_0)}{\varepsilon_N^2 \sqrt{N}}, \end{aligned} \quad (16)$$

for any sequence $\varepsilon_N > 0$ that tends to 0, where $R_\infty = 2 \sup_{f \in \mathcal{G}_0} \|f\|_\infty$, $R_2 = 2 \sup_{f \in \mathcal{G}_0} \|f\|$, $J_0(2R_2, \mathcal{G}_0)$ is the entropy as (2.2) in van de Geer (2014) for the function class \mathcal{G}_0 , and the constant C_B depends on the supremum norm of f_B and the class \mathcal{G} .

When $\mathcal{G}_0 = \mathcal{G}$, the upper bound in (16) can be simplified to

$$\frac{1024}{\varepsilon_N^4} \cdot \left\{ \frac{\|f_B\|_{TV}^2}{K+3} + C_B \frac{2^K \log^2 N \log(Nd)}{N} \right\} + \frac{32R_\infty J_0(2R_2, \mathcal{G})}{\varepsilon_N^2 \sqrt{N}}, \quad (17)$$

and the constant C_B only depends on the total variation of f_B .

Proof See Appendix D. ■

The right-hand side of (16) decomposes the first term inside the infimum into three components: the possible approximation error $\|f_B - g\|^2$ induced by finite depth K ; the total variation caused by the tree approximant g ; the decaying term showing that d can grow exponentially without losing the consistency of a CART fit. The second term bounds the difference between the empirical norm and the ℓ_2 norm.

Theorem 10 holds for any sample size. This theorem yields asymptotic rates by letting N diverge; we can see that the obtained rate ε_N is not faster than $N^{-1/4}$, which is much slower than that obtained in the following Theorem 13. Substituting $\varepsilon_N \asymp O(N^{-1/4-\delta})$ yields the following consistency result for ranking.

Corollary 11 *Under the same conditions as in Theorem 10, if we assume that the depth $K = K_N$ of the tree grows with the sample size N in such a way that*

$$\|f_B\|_{TV}^2 \asymp o\left(\varepsilon_N^4 \sqrt{K}\right), \frac{2^K \log^2 N \log(Nd)}{N} \asymp o(\varepsilon_N^4),$$

where $\varepsilon_N^4 N \rightarrow \infty$ (i.e., $\varepsilon_N \asymp O(N^{-1/4-\delta})$ for $\delta > 0$) as $N \rightarrow \infty$, then there holds

$$\lim_{N \rightarrow \infty} \mathbb{E}_{(\mathcal{X}^{(N)}, \mathcal{Y}^{(N)})} (|\mathbf{T}(r_B) - \mathbf{T}(r_{c,K})|) \rightarrow 0.$$

Remark 12 *The assumptions $\|g\|_{TV}^2 \asymp o(\varepsilon_N^2 \sqrt{K})$, $\frac{2^K \log^2 N \log(Nd)}{N} \asymp o(\varepsilon_N^2)$ are parallel to the assumptions imposed by Corollary 4.4 in Klusowski and Tian (2024).*

The next result shows that, under conditions, BART has a posterior concentration close to f_B if the y_i 's are generated by (1). We consider a fixed and regular design as described in Definition 7.1 of Ročková and Saha (2019) or Definition 3.3 in Ročková and van der Pas (2020). In the context of Ročková and van der Pas (2020), a *regular design* refers to a fixed dataset where the diameters of the cells in a k -d tree partition are controlled and relatively uniform. Specifically, the maximal diameter in the partition components should not be significantly larger than a typical diameter. An example of a regular dataset would be a fixed design on a regular grid, where the points are evenly spaced and no cells have an excessive spread of points compared to others. In contrast, a dataset with highly skewed or isolated points in certain directions might not meet the regularity condition.

We use the probability measure corresponding to responses generated using the Bayes scoring function f_B in model (1), which implies that the response should be considered evaluated at these fixed inputs with random noise.

Theorem 13 (*Fixed design*) *Assume that the Bayes scoring function f_B is ν -Holder continuous for $\nu \in (0, 1]$, with the norm $\|f_B\|_\infty \lesssim \log^{1/2} N$ and a regular design over the set $\mathcal{X}^{(N)} = \{\mathbf{x}_1, \dots, \mathbf{x}_N\} \subset \mathbb{R}^d$ where $d \lesssim \log^{1/2} N$. Let the function class \mathcal{F} be defined as a set of additive simple functions as described in (3) of Ročková and Saha (2019). Consider the BART prior with a fixed number of trees and node splitting probability $p_{\text{split}}(\eta) = \alpha^{\text{depth}(\eta)}$ for a node η and $\alpha \in [\frac{1}{N}, \frac{1}{2}]$. Then, the following contraction for BART posterior \prod holds for the resulting posterior distribution and the BART induced ranking functions r_f from (1):*

$$\prod (f \in \mathcal{F} : \mathbf{T}(r_B) - \mathbf{T}(c_f) > M_N \varepsilon_N | y_1, \dots, y_N) \rightarrow 0$$

in probability measure of the y_1, \dots, y_N , where $\varepsilon_N = N^{-\alpha/(2\alpha+d)} \log^{1/2} N$, and for any sequence $M_N \rightarrow \infty$, as the sample size $N \rightarrow \infty$ and the dimensionality $d \rightarrow \infty$.

Proof See Appendix E. ■

Remark 14 *The Bayes scoring function $f_B(\mathbf{x}_j)$ always exists (see Theorem 1 in Cossock and Zhang (2006)). Theorem 13 indicates that as we fit BART with an increasing number of samples \mathcal{X} satisfying a regular design, the resulting posterior will concentrate around the Bayes scoring function. Unlike the finite-sample result for a single binary tree established in Theorem 10, Theorem 13 provides an asymptotic result concerning the posterior distribution of BART.*

Building on our previous discussions from a ranking perspective, we can summarize the findings as follows: Locally, at each split, the partitions are most likely divided into rank-consistent groups, but within each partition, no ranking is available since the scoring function remains constant within each partition. Globally, in the asymptotic behavior of BART, the posterior tends to concentrate near the Bayes scoring functions that minimize the L_2 (hence \mathbf{T} metric) error. Meanwhile, CART also achieves consistent ranking performance, with finite-sample bounds available.

5 Concordant Divergence

We now shift to leveraging the ranking perspective to study symbolic feature selection as illustrated in Example 1. Although tree-based methods have demonstrated strong finite-sample performance in distinguishing between symbolic features that are transformations of one another, it remains elusive since the existing theory, viewed through the lens of nonparametric variable selection, is unaffected by such transformations. In this section, we extend our previous analysis to uncover additional characteristics of tree-based methods. Building on these insights, we introduce a *concordant divergence* statistic, \mathcal{T}_0 , which can evaluate feature mappings.

The local split analysis in previous sections has provided some insight into tree-based methods when transformations are involved. Section 3.1 shows that the oracle partition, relevant only to the ranks of responses y 's, may not be attainable with a single split along the input domain, unless there is monotonicity along one coordinate. Section 3.2 compares two piecewise transformations in a relative sense. Next, we first present another local-level observation before extending the ranking perspective to study a general mapping g in an absolute sense, moving beyond local splits.

Lemma 15 *(Magnitude of swaps) Under the same assumptions as in Lemma 1, we suppose that the only reversed pairs are (y_α, y_γ) and (y_β, y_γ) where $y_\alpha > y_\gamma, y_\beta > y_\gamma$ and both $y_\alpha, y_\beta \in P_1$ but $y_\gamma \in P_2$. If $y_\alpha > y_\beta > y_\gamma$, then the swap for the pair (y_α, y_γ) reduces the loss (10) more than the swap for the pair (y_β, y_γ) .*

Proof See Appendix F. ■

Lemma 1 highlights the effect of the magnitude of the responses. In particular, we might prioritize the swapping of a reverse pair with a larger “size”, i.e., the difference between the responses y in the reversed pair. It is possible that there exist two reversed pairs with the same “sizes”. However, with our assumption that both inputs and responses are continuous, it is with zero probability that we have two reverse pairs such that their magnitudes are identical.

Based on the discussion of tree-like models for the univariate case (Lemmas 1 and 15), we can summarize the principle behind feature selection as follows: it selects the feature mapping g that takes \mathbf{x} into transformed images \mathbf{z} that have the most similar rankings as the response y . The discrepancies between these rankings can be described by the “gaps” between ordered statistics of

y 's. Motivated by Lemma 15, we develop \mathcal{T}_0 to evaluate arbitrary feature mapping θ :

$$\begin{aligned} \mathcal{T}_0(\theta) = \sum_{\pi} \frac{2|y_{\pi(1)} - y_{\pi(2)}|}{n(n-1)} \cdot \{ & \mathbf{1}(\theta(\mathbf{x}_{\pi(1)}) \geq \theta(\mathbf{x}_{\pi(2)})) \cdot \mathbf{1}(y_{\pi(1)} < y_{\pi(2)}) \\ & + \mathbf{1}(\theta(\mathbf{x}_{\pi(1)}) < \theta(\mathbf{x}_{\pi(2)})) \cdot \mathbf{1}(y_{\pi(1)} \geq y_{\pi(2)}) \}, \end{aligned} \quad (18)$$

where the summation takes over all permutations of length 2 as $(\pi(1), \pi(2))$ with $\pi(1), \pi(2) \in \{1, \dots, n\}$. Guided by the ranking behavior induced by tree methods, $\mathcal{T}_0(\theta)$ evaluates a symbolic feature $\theta(\mathbf{x})$ by measuring to what extent it can recover the order of y 's. In particular, if $\theta(\mathbf{x}(i)) < \theta(\mathbf{x}(j))$, we have a zero summand; otherwise, we will have a non-negative summand $|y(i) - y(j)|$. A larger $\mathcal{T}_0(\theta)$ indicates more discrepancy between the rankings of $\theta(\mathbf{x})$ and y , and we accumulate all these discrepancies. Note that despite the intimate connection with the ranking performance of tree methods, to use this divergence, we do not need to consider a tree model, but simply a finite number of samples.

Remark 16 *The \mathcal{T}_0 is similar to Kendall's tau (Hollander et al., 2013) but with the additional non-negative multiplier, $|y_{\pi(1)} - y_{\pi(2)}|$, representing "the magnitude of swaps". It involves both the ranks and the actual values of the responses y . This \mathcal{T}_0 is also not the same as linear correlation coefficients. Daniels (1944) (in Section 5) stated that the linear correlation coefficients ρ satisfy $\rho_{\theta x, y} = \rho_{\theta x, x} \rho_{x, y}$ for any transformation θ , which means that the correlation $\rho_{\theta x, y}$ cannot increase beyond $\rho_{x, y}$ since $\rho_{\theta x, x} \leq 1$. However, the behavior of \mathcal{T}_0 is not constrained in the same way when transformations are introduced.*

For inactive variables, we want to exclude both the variable itself and all its transformations. From the following definition, it is clear that any transformation of inactive variables will also remain inactive.

Definition 17 *(Inactive variable) A feature $\mathbf{X}_k \in \mathbb{R}$ of a continuous input variable $\mathbf{X}, k \in \{1, \dots, d\}$ is called inactive (for function f as in (1)), if the distribution of y is independent of the distribution of $f(\mathbf{X}_k)$.*

Considering a random design where each row of \mathbf{X} is drawn independently from a distribution, we have the following properties for \mathcal{T}_0 when evaluating transformations of \mathbf{X}_k :

Proposition 18 *(i) if \mathbf{X}_k is an inactive variable, then $\mathbb{E}_{\mathbf{X}_k, \mathbf{y}} \mathcal{T}_0(f) \not\rightarrow 0$ as $n \rightarrow \infty$.
(ii) if there exists a transformation $\theta = g$ such that $g(\mathbf{x}_1) \geq g(\mathbf{x}_2) \Leftrightarrow y_1 \geq y_2$, then $\mathbb{E}_{\mathbf{X}, \mathbf{y}} \mathcal{T}_0(g) = 0$.*

Proof See Appendix G. ■

These two results establish the fact that \mathcal{T}_0 will never prefer a mapping consisting of an inactive variable (Proposition 18, i), unless that mapping is a "fake interpolator" for the given finite sample (Proposition 18, ii and Example 5). In an extreme case where all variables are inactive, that is, none of the coordinates in \mathbf{X} determine the value of y , part (i) of the proposition implies that \mathcal{T}_0 will not be zero. This means that if we take $g = \text{id}$, then such an identity mapping is not an interpolator (see Example 5). However, this does not rule out the possible existence of an interpolator $g \neq \text{id}$ such that g "reorganizes" \mathbf{X} and y in a concordant way, even if \mathbf{X} are completely inactive.

As we do not actually have to use a tree structure when computing \mathcal{T}_0 , this gives us convenience in practice. In symbolic feature selection, we will calculate the correlation $\mathcal{T}(y(\mathbf{z}))$ between the response y_i and each coordinate of \mathbf{z}_i to find useful features (i.e., correlation between the \mathbf{y} vector and the q columns of \mathbf{z} matrix).

Example 8 (Power of \mathcal{T}_0) In Figure 4, we present 5 different feature mappings $\theta_1, \dots, \theta_5$ and compute their pairwise correlations and \mathcal{T}_0 and compare its performance to other correlations. For ease of comparison, we use log-scale for \mathcal{T}_0 and $[0,1]$ scale for the other correlations. We will expect the divergence to be close to 0, indicating dependence between the sample \mathbf{x} and $\theta_i(\mathbf{x})$ to various extents (i.e., $\mathcal{T}_0 = 0$ as in Proposition 18 (ii)). Since $\theta_1 = \mathbf{x}$ coincide with $\theta_2, \dots, \theta_5$ to different extents, we also want the correlation reflect the degree of dependence.

The Chatterjee (2021)’s correlation coefficient $\xi_n(\mathbf{X}, \mathbf{y})$ and the \mathcal{T}_0 are both asymmetric and measure both capture non-linear dependencies between pairs of random variables, particularly non-linear dependencies. The $\xi_n(\mathbf{X}, \mathbf{y})$ rearranges data pairs based on sorted values and computes rank-based statistics, making it sensitive to changes in the data’s distribution and structure. On the other hand, \mathcal{T}_0 is a permutation-based measure that evaluates the sum of contributions from all possible pairs of data points, considering differences in values and their rankings. This exhaustive approach in computing divergence is robust against outliers and provides a detailed understanding of pairwise dependencies. However, it is computationally intensive due to the reliance on permutations, especially for moderate to large datasets.

From Figure 4, we can observe that classic correlations like Pearson, Spearman, and Kendall cannot detect the functional dependence between \mathbf{x} and the other θ_i ’s regardless of the signal-to-noise ratio, which is proportional to $1/\sigma^2$. However, the Chatterjee (2021) correlation and \mathcal{T}_0 are capable of capturing this dependence when the signal-to-noise ratio is high and the sample size is sufficiently large ($N = 50$). In addition, we may also observe that compared to Chatterjee correlation, \mathcal{T}_0 will not falsely detect functional dependence when the signal-to-noise ratio is low, even with only $N = 50$. Chatterjee correlation seems to stumble when the sample size is limited. θ_1 and the rest $\theta_2, \dots, \theta_5$ have different degree of overlapping, which is reflected by the magnitude of \mathcal{T}_0 (when noise variance is small), but not by the other correlations.

This example elucidates the behavior of various selection criteria when applied to four distinct features generated from the same input. In contrast to Pearson, Spearman and Kendall correlation, which measure linear and ordinal association respectively, the \mathcal{T}_0 statistic demonstrates an effective approach. It does not erroneously filter out the correct function when compared to the correlations between the true function and the different features $\theta_i \mathbf{x}$. As shown in the experimental results in Figure 4, only \mathcal{T}_0 can detect the functional dependence and being sensitive to signal-to-noise ratio; and this makes \mathcal{T}_0 a suitable correlation of detecting even different sampling plans. This exemplifies \mathcal{T}_0 ’s utility in feature selection, where the goal is to maintain the true influential features.

6 Experiments

In this section, we conduct simulations to assess the performance of the proposed \mathcal{T}_0 divergence for selecting variables and symbolic expressions, and lend support to the theoretical results in preceding sections. We expect that the concordant divergence statistics, which is motivated as derived from the discussion that “tree-based splits are attempting to match the rankings of \mathbf{z} and \mathbf{y} ”, will behave similarly to the tree-based methods, on these symbolic regression tasks.

6.1 AUC for feature selection

Continuing the discussion in Example 1 We consider a 3-dimensional input variables $(x_1, x_2, x_3) \in [0, 1]^3$ and the following model

$$y = 2x_1^3 + 5x_3 + 10 + \epsilon, \tag{19}$$

where $\epsilon \sim N(0, \sigma^2)$. With sample size n , we generate an $n \times 3$ matrix \mathbf{X} for input variables using uniform random variables, and the corresponding \mathbf{y} using (19). We consider two architectures

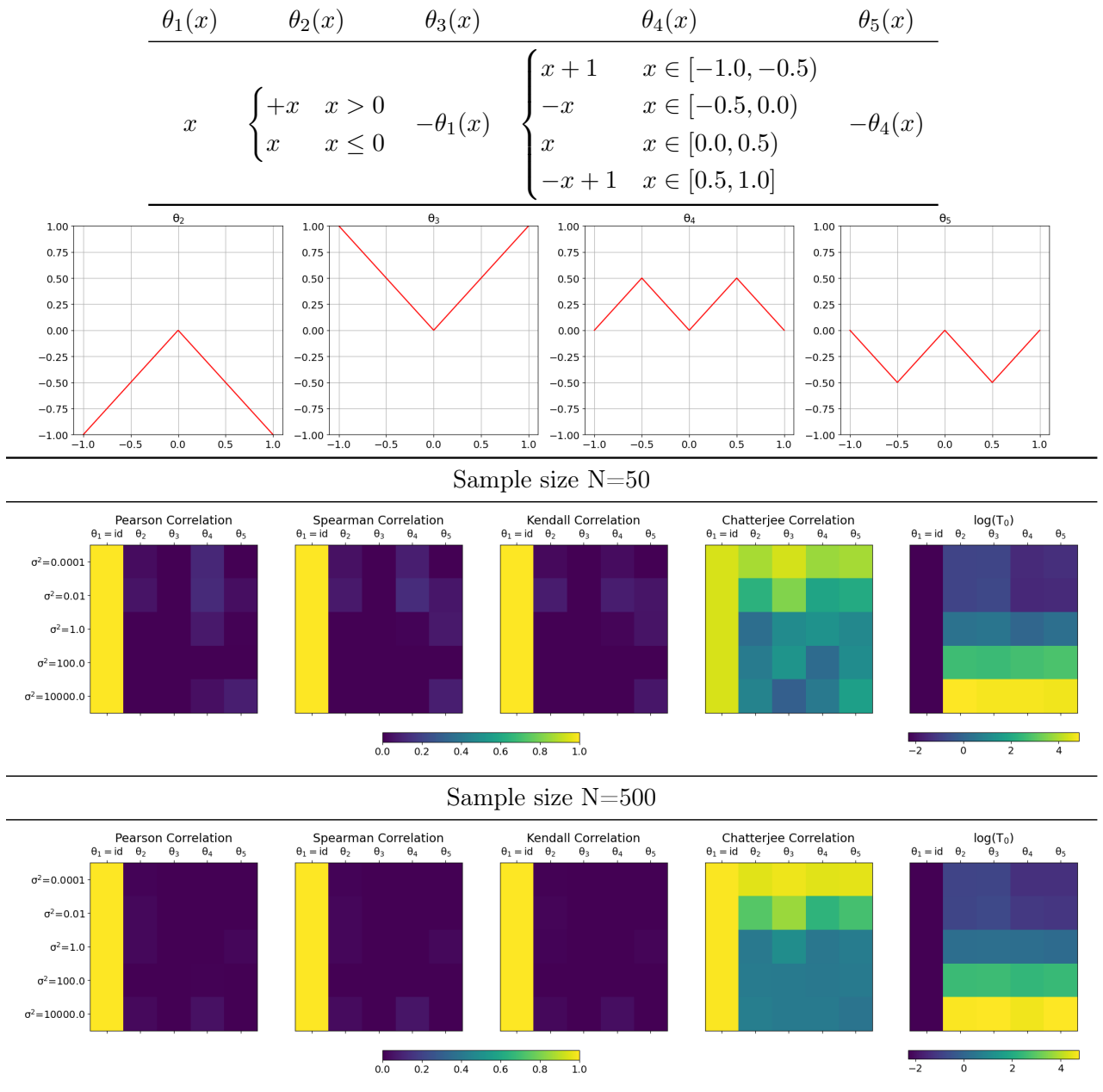


Figure 4: Correlation between \mathbf{x} and $\mathbf{y} = \theta_i(\mathbf{x})$ for $i = 1, \dots, 5$. The expression and figure for each θ_i are reported in the top two rows in the table. Left to Right (in the 3rd and 4th rows): Chatterjee correlation (Chatterjee, 2021), absolute Pearson correlation, absolute Spearman correlation and absolute Kendall correlation, $\log(\mathcal{T}_0)$. The \mathcal{T}_0 is shown on a log-scale for better comparison. We generate an equally spaced \mathbf{x} on $[-1, 1]$ with sample size $N = 50$ (3rd row) and $N = 500$ (4th row). Gaussian noises with variance σ^2 are added to $\theta_i(\mathbf{x})$.

for generating transformations: $\mathcal{O}_{A_u}^{(2)} = \mathcal{O}_u \circ \mathcal{O}_b$ and $\mathcal{O}_{A_b}^{(2)} = \mathcal{O}_b \circ \mathcal{O}_u$, where $\mathcal{O}_u = \{id, x^3\}$ and $\mathcal{O}_b = \{+, \times\}$. The design matrix for each architecture has the following dimensionality:

	$\theta_1(x)$	$\theta_2(x)$	$\theta_3(x)$	$\theta_4(x)$
	x	$2 \sin(x)$	$2 \sin(7x)$	$\sin(x)$
BART Global Max	18.0	10.0	10.0	0.0
BART Local	29.0	29.0	25.0	0.0
Pearson	0.0	100.0	0.0	0.0
Kendall	100.0	0.0	0.0	0.0
\mathcal{T}_0	100.0	100.0	100.0	0.0
	x	$\sin(4x + 0.2)$	$\sin(4x + 0.1)$	$\sin(4x)$
BART Global Max	0.0	0.0	5.0	64.0
BART Local	0.0	0.0	9.0	83.0
Pearson	0.0	0.0	0.0	100.0
Kendall	0.0	0.0	0.0	100.0
\mathcal{T}_0	0.0	0.0	0.0	100.0
	x	$\cos(x)$	$\sin(2x)$	$\sin(x)$
BART Global Max	4.0	5.0	6.0	5.0
BART Local	7.0	11.0	13.0	13.0
Pearson	0.0	0.0	0.0	100.0
Kendall	100.0	0.0	0.0	0.0
\mathcal{T}_0	100.0	0.0	100.0	100.0
	x	$\sin(4x)$	$\sin(6x)$	$\sin(5x)$
BART Global Max	0.0	16.0	0.0	61.0
BART Local	1.0	29.0	0.0	68.0
Pearson	0.0	0.0	0.0	100.0
Kendall	0.0	0.0	0.0	100.0
\mathcal{T}_0	0.0	0.0	0.0	100.0

Table 1: The inclusion percentage, as an empirical approximation to the inclusion probability, by methods BART (`bartMachine` R package ($m = 50$)), \mathcal{T}_0 , Pearson’s correlation and Kendall’s tau between $x, \theta x$ are provided for comparison. The true signal θ_4 is highlighted in bold, and all experiments are done with $\mathbf{x} \sim N(0, 1)$ with sample size 500.

1. For $\mathcal{O}_{A_u}^{(2)}$, after the first layer of binary operations, we have $2(C_3^2 + C_3^1) = 12$ different features and a $n \times 12$ matrix. Then, we take this $n \times 12$ matrix as the input of the next layer of unary operations and produce $C_2^1 \times 12 = 24$ different features and a $n \times 24$ matrix.
2. For $\mathcal{O}_{A_b}^{(2)}$, similarly to the calculation above, the first layer of unary operations gives $C_2^1 \times 3 = 6$ features, and the second layer of binary operations give $2(C_6^2 + C_6^1) = 42$ features.

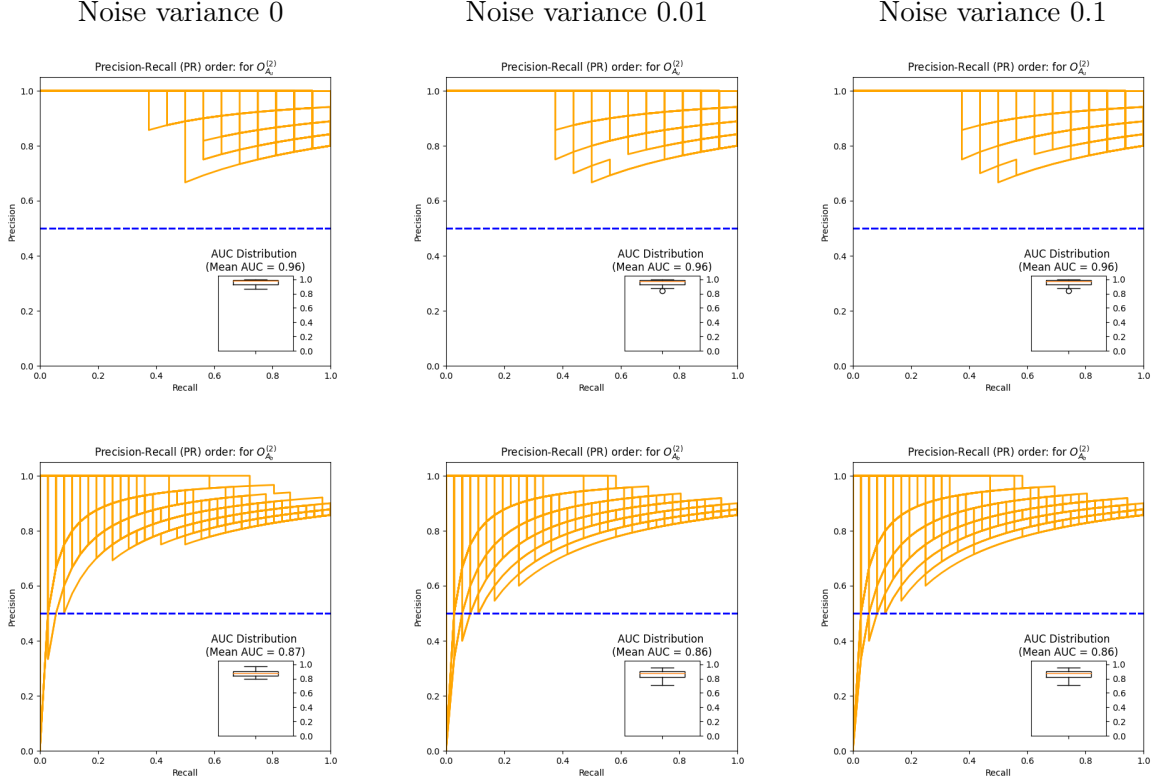


Figure 5: We illustrate the PR curves from 50 repeats ($n = 100$) of a 2-layer symbolic regression with $\mathcal{O}_u = \{id, x^3\}$ and $\mathcal{O}_b = \{+, \times\}$. The true signal is (19) with no noise. The first row corresponds to the architecture of $\mathcal{O}_{A_u}^{(2)}$ and the second row corresponds to the architecture of $\mathcal{O}_{A_b}^{(2)}$. We provide the boxplot to show the AUC values amongst 50 repeats.

For $\mathcal{O}_{A_u}^{(2)}$		For $\mathcal{O}_{A_b}^{(2)}$			
$x_1 + x_1$	$x_1 \times x_3$	$x_1 + x_1$	$x_1 + x_3$	$x_1^3 + x_3$	$x_3 + x_3^3$
$(x_1 + x_1)^3$	$(x_1 \times x_3)^3$	$x_1 \times x_1$	$x_1 \times x_3$	$x_1^3 \times x_3$	$x_3 \times x_3^3$
$x_1 \times x_1$	$x_3 + x_3$	$x_1 + x_1^3$	$x_1 + x_3^3$	$x_1^3 + x_3^3$	$x_3^3 + x_3^3$
$(x_1 \times x_1)^3$	$(x_3 + x_3)^3$	$x_1 \times x_1^3$	$x_1 \times x_3^3$	$x_1^3 \times x_3^3$	$x_3^3 \times x_3^3$
$x_1 + x_3$	$x_3 \times x_3$	$x_1^3 + x_1^3$	$x_1^3 + x_1^3$	$x_3 + x_3$	
$(x_1 + x_3)^3$	$(x_3 \times x_3)^3$	$x_1^3 \times x_1^3$	$x_1^3 \times x_1^3$	$x_3 \times x_3$	

Table 2: Correct features for the problem (19) as they *only* contains x_1 , x_3 , or their transforms.

The goal of symbolic regression is to select features from the $n \times 24$ matrix (if $\mathcal{O}_{A_u}^{(2)}$) or $n \times 42$ matrix (if $\mathcal{O}_{A_b}^{(2)}$) given data.

The true signal in (19) uses only x_1 and x_3 . For evaluation, we consider a feature to be “correct” as long as it *only* contains x_1 , x_3 , or their transforms (as listed out in Table 2). To obtain a useful ROC curve, we first create an array called `ground_truth` of size N_{total} , initialized with zeros. We assign $N_{true}(= 1)$ true feature to the ground truth array by setting its corresponding element to 1. Next, we create an array called `predicted_scores` of size N_{total} , containing random scores for each feature. We then assign the highest $N_{selected}$ predicted scores from our BART selection procedure to the selected features by sorting the scores and assigning the top $N_{selected}$ values to the selected

feature indices. We use $N_{selected} = 3$ in this experiment to indicate that there may be x_1, x_3 and the constant intercept (which is included by default) in (6.1) will be correctly selected.

Finally, we plot the performance curve¹ along with the reference diagonal line representing the performance of a random classifier. According to the criterion where we consider a feature to be “correct” as long as it *only* contains x_1, x_3 , we can examine each of the (24 or 42) features and label them as 1 if “correct”; as 0 if not. With this manually examined ground truth label, we also compare the $N_{selected} = 3$ labels to this ground truth, we can compute the precision-recall curve and its AUC. The AUC value is shown in the legend, providing a measure of the performance of our feature selection method. The higher the AUC, the better our method is at identifying the true feature among the selected features. In symbolic regression, we focus on keeping the correct signals involving active variables, metrics like AUC for Precision-Recall curve is more appropriate for evaluating the performance of each method than the usual TDR/FDR AUC, as we provided in Figure 5. A high PR AUC indicates that the model achieves both high recall and high precision, maintaining a good balance, especially when a positive class is of great interest or when negative examples outnumber positive ones.

From Figure 5, we can observe that as the noise variance increases, the AUC decreases. It is also of interest to observe that in the $\mathcal{O}_{A_u}^{(2)}$ setting, the AUC is higher than that of the architecture of $\mathcal{O}_{A_b}^{(2)}$. This lends support to the architecture design in Ye et al. (2024) that the binary operator should be introduced as the first alternating layer.

6.2 Comparison against other methods

Furthermore, we use the same experiment to compare the performance of different model-based feature selection methods, and our \mathcal{T}_0 using the signal (19). We select the features using \mathbf{y} with different additive noise variances and the corresponding \mathbf{X} from $\mathcal{O}_{A_u}^{(2)}$ (24 features) or $\mathcal{O}_{A_b}^{(2)}$ (42 features) architectures. For comparison, we include LASSO (`glmnet == 4.1 – 8`, Hastie et al. (2009) with lambda chosen by default cross-validation (`lambda=-1`)), SCAD (`ncvreg == 3.14.1`, Fan et al. (2014)) and step-wise subset selection using linear models (LMSTEPWISE, `leaps :: regsubsets == 3.1`) as competitors of model-based feature selections methods. Our \mathcal{T}_0 in (18) inspired by ranking perspective from BART is the only method that is not model-based. In what follows, our concern is the correct feature selection instead of predictive performance. Thus, we simply use the same dataset for selecting the features.

Previously, we observed in Example 8 that \mathcal{T}_0 behaves differently than classical correlation coefficient. In this set of experimental results in Figure 6, we display the *average inclusion probability* (AIP) as an approximation to the frequency of features being selected, since \mathcal{T}_0 is not a formal feature selection method that can be evaluated by AUC curve, yet we still want to see how well it performs when we select the feature with smallest concordant divergence statistics. All those features *only* contains x_1, x_3 or their transforms (of any kind) are considered correct if selected. Then we repeat the experiment for 50 different random \mathbf{X} and computed the frequency that each of these correct features are selected. Then we sum up these probabilities and divide by $N_{selected} = 3$, as our AIP metric in Figure 6. That means we ask each method to pick $N_{selected} = 3$ features among all possible features for 50 times, and AIP represents the average probability that these features are all correct. The higher AIP means more correct features are chosen in this configuration of sample size, noise variance, and method.

1. We calculate the false positive rate (FPR) and true positive rate (TPR) at various thresholds using the `roc_curve` function from `sklearn.metrics`, which takes the ground truth labels and predicted scores as input. The AUC value is computed using the `auc` function, which calculates the area under the ROC curve using the trapezoidal rule.

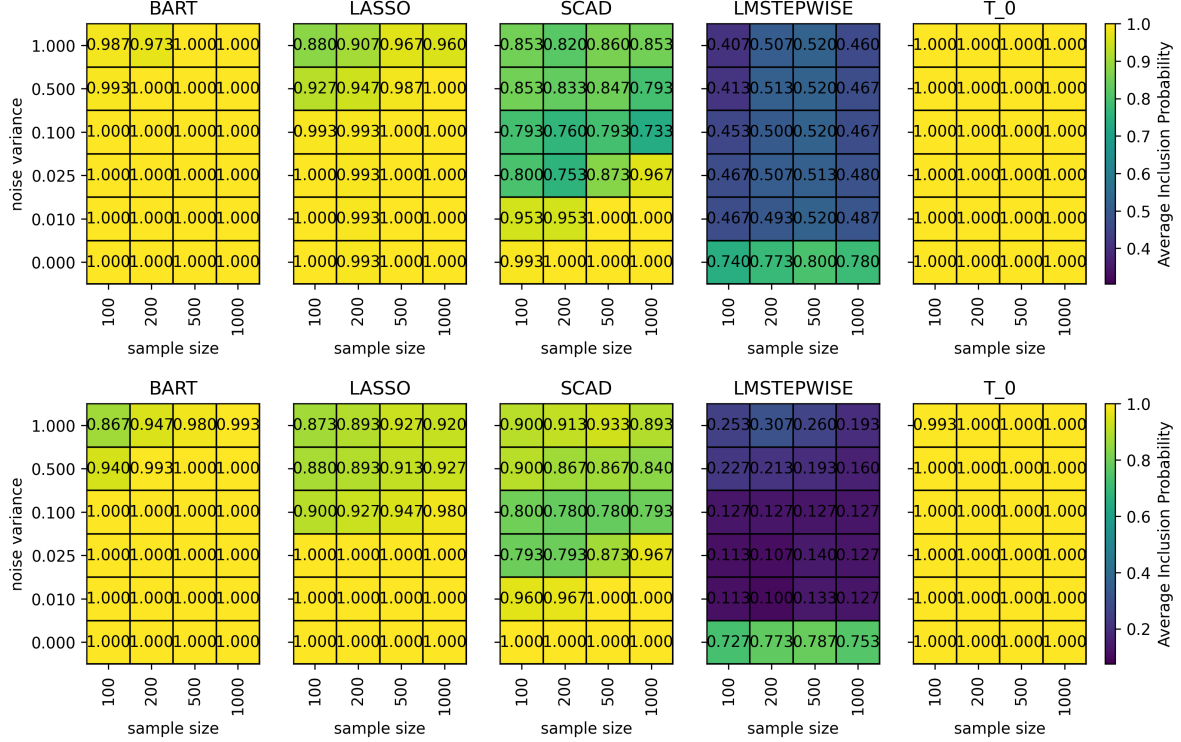


Figure 6: We illustrate the average inclusion probabilities from 50 repeats of a 2-layer symbolic regression with $\mathcal{O}_u = \{id, x^3\}$ and $\mathcal{O}_b = \{+, \times\}$. The true signal is (19). The first row corresponds to the architecture of $\mathcal{O}_{A_u}^{(2)}$ and the second row corresponds to the architecture of $\mathcal{O}_{A_b}^{(2)}$.

It is not hard to see that both BART and \mathcal{T}_0 are performing extremely well for low noise variances, followed by LASSO. LASSO and SCAD are behaved surprisingly well in this 2-layer example perhaps due to the relatively small number of features, in contrast to the Ye et al. (2024)’s setting where a much large number of features need to be screened. However, the low AIP associated with linear model stepwise selection (LMSTEPWISE) is clearly not suitable for this scenario for $\mathcal{O}_{A_u}^{(2)}$ nor $\mathcal{O}_{A_b}^{(2)}$. One step further, we point out that \mathcal{T}_0 is the fastest method, even if it involves summation over permutations, followed by LASSO. While BART has the benefit of providing uncertainty quantification and higher selection power, it is among the slower methods due to its MCMC sampling step.

Concurrently, we also test these nonparametric methods on classic ODE-Strogatz repository for symbolic regression dataset as an example of “ground-truth regression problems” (La Cava et al., 2021). However, we did not intend to compete with the formal symbolic regression methods but focus on the feature selection accuracy like above. In this experiment, we use different orders of symbolic compositions (e.g., ub, ubb) instead of alternating layers to ensure that the correct composition of symbols can be obtained through the architecture. In addition to different layers, we also use different sets of binary and unitary operators to have better generality. The LMSTEPWISE cannot work properly due to the >100 co-linear features in these examples. Since all expressions contain x_1 (x variate in raw data) and x_2 (y variate in raw data), we bring in a more stringent criteria: all those features *only* contains x_1, x_3 and their correct transforms are considered correct.

To make the comparison fair, we enforce that the regression does not attempt to estimate relevant coefficients for symbolic terms but look at the selected features among all possible expressions. From

Table 3, we can observe that for simple ODEs (vdp2), all four methods behave reasonably well. However, when we study additive signals with different magnitudes (glider1, vdp1), the LASSO and SCAD do not recognize the correct format. BART behaves bad too, while \mathcal{T}_0 actually identify features that coincide with the original ODE signal better. For complicated composition (glider2), it seems that all methods except SCAD and \mathcal{T}_0 work pretty well, even if coefficient estimates are not allowed.

Symbolic composition order

dataset	truth	\mathcal{O}_u	\mathcal{O}_b	order
glider1	$-0.05x_1^2 - \sin(x_2)$	$\{\sin(x), x^2\}$	$\{+, -\}$	ub
glider2	$x_1 - \cos(x_2)/x_1$	$\{\cos(x), \text{id}\}$	$\{-, /\}$	ubb
vdp1	$-10/3x_1^3 + 10/3x_1 + 10x_2$	$\{x^3\}$	$\{+, -\}$	ubb
vdp2	$-x_1/10$	/	/	/

Results by each method with noise variance 0.100

method	glider1	glider2	vdp1	vdp2
BART	x_2^2	$\cos(x_2)/x_2 - x_1 - x_2$	$x_1^3 + x_2^3 - x_2^3$	x_2
LASSO	$\sin(x_1)/\sin(x_2)$	$\cos(x_2)/x_2 - x_1 - x_2$	x_2^3	x_2
SCAD	x_2^2	x_1	x_2^3	x_2
\mathcal{T}_0	$\sin(x_1) - \sin(x_2)$ or $\sin(x_1) - x_1$	$x_1 - \cos(x_1)/\cos(x_2) - x_1$	$x_1^3 - x_2^3 - x_1^3$ or x_2	x_2

Table 3: The most frequently selected expressions from datasets ($n = 400$) in the ODE-Strogatz repository <https://github.com/lacava/ode-strogatz>, as generated by using the first principles physical models. The LMSTEPWISE (linear model with step-wise selection) runs into error due to the high co-linearity in the input of these datasets.

7 Discussion and Future work

Tree-based methods are highly effective for a wide range of real-world tasks. The current understanding of this effectiveness often relies on asymptotic analysis or heuristics. While advancements in these two directions are both useful, they yield a substantial gap that calls for a formal investigation of tree-based methods that can generalize and closely link to their empirical success. In this paper, we develop a comprehensive ranking perspective for understanding tree-based methods. We provide a series of finite-sample analyses concerning the interplay between splits and ranking, covering local splits, single trees, and tree ensembles. Asymptotics results are also established when we evaluate selected tree-based methods using their ranking performance. One particular application is symbolic feature selection in the presence of transformations of input variables, a crucial step in symbolic regression that the empirical success of tree-based methods has only been observed re-

cently. Our ranking perspective leads to insights when comparing transformations and also provides new divergence statistics as a method to select symbolic features.

The motivation for this work was to develop a better understanding of a broad class of tree-based methods through ranking. A future objective is to provide a foundation for more model structures to which tree-based methods can be applied, including classification, non-Gaussian error assumptions and non-standard inputs (Luo and Ma, 2024; Luo et al., 2024). The ranking perspective is presumably more robust to model misspecification, which might help explain the robustness of tree methods in real-world applications. Similarly, Cl  men  on et al. (2008) highlighted that ranking theory, when extended beyond two items, significantly depends on the designated loss, marking an interesting area for further research when the principal decision ratio τ is defined by other norms (e.g., L^1). Finally, our ranking perspective on tree methods can be expanded to provide uncertainty quantification for ranking.

Acknowledgment

HL thanks for Mikael Vejdemo Johansson for kindly providing computational resource in pilot experiments. HL was supported by the Director, Office of Science, of the U.S. Department of Energy under Contract DE-AC02-05CH11231, and DE-FOA-0002958. HL is also supported by NSF grant DMS 2412403. ML’s research was partially supported by NSF grant DMS/NIGMS-2153704.

References

- Abhineet Agarwal, Yan Shuo Tan, Omer Ronen, Chandan Singh, and Bin Yu. Hierarchical Shrinkage: Improving the Accuracy and Interpretability of Tree-based Models. In *International Conference on Machine Learning*, pages 111–135. PMLR, 2022.
- Mirela Andronescu and Mark Brodie. Decision Tree Learning using a Bayesian Approach at Each Node. In *Advances in Artificial Intelligence: 22nd Canadian Conference on Artificial Intelligence, Canadian AI 2009 Kelowna, Canada, May 25-27, 2009 Proceedings 22*, pages 4–15. Springer, 2009.
- Susan Athey, Julie Tibshirani, and Stefan Wager. Generalized random forests. *The Annals of Statistics*, 47(2):1148 – 1178.
- Justin Bleich, Adam Kapelner, Edward I George, and Shane T Jensen. Variable Selection for BART: an Application to Gene Regulation. *The Annals of Applied Statistics*, 8(3):1750–1781, 2014. Publisher: Institute of Mathematical Statistics.
- Leo Breiman, Jerome Friedman, Richard A. Olshen, and Charles J. Stone. *Classification and Regression Trees*. Routledge, 1987.
- Randal E Bryant. Symbolic Boolean Manipulation with Ordered Binary-decision Diagrams. *ACM Computing Surveys (CSUR)*, 24(3):293–318, 1992.
- Sourav Chatterjee. A New Coefficient of Correlation. *Journal of the American Statistical Association*, 116(536):2009–2022, 2021.
- Hugh A Chipman, Edward I George, and Robert E McCulloch. Bayesian CART Model Search. *Journal of the American Statistical Association*, 93(443):935–948, 1998.
- Hugh A Chipman, Edward I George, and Robert E McCulloch. Bayesian Treed Models. *Machine Learning*, 48:299–320, 2002.
- Hugh A. Chipman, Edward I. George, and Robert E. McCulloch. BART: Bayesian Additive Regression Trees. *The Annals of Applied Statistics*, 4(1):266–298, 2010.
- Stéphan Cléménçon, Gábor Lugosi, and Nicolas Vayatis. Ranking and Empirical Minimization of U-statistics. *The Annals of Statistics*, 36(2), 2008.
- Stéphan Cléménçon and Sylvain Robbiano. The TreeRank Tournament Algorithm for Multipartite Ranking. *Journal of Nonparametric Statistics*, 27(1):107–126, 2015.
- Stéphan Cléménçon and Nicolas Vayatis. On Partitioning Rules for Bipartite Ranking. In *Artificial Intelligence and Statistics*, pages 97–104. PMLR, 2009.
- Stephan Cléménçon and Robin Vogel. On Tree-based Methods for Similarity Learning. In *International Conference on Machine Learning, Optimization, and Data Science*, pages 676–688. Springer, 2019.
- Stéphan Cléménçon, Marine Depecker, and Nicolas Vayatis. Adaptive Partitioning Schemes for Bipartite Ranking. *Machine Learning*, 83(1):31–69, 2011.
- David Cossock and Tong Zhang. Subset ranking using regression. In *Learning Theory: 19th Annual Conference on Learning Theory, COLT 2006*, pages 605–619. Springer, 2006.

- H. E. Daniels. The Relation Between Measures of Correlation in the Universe of Sample Permutations. *Biometrika*, 33(2):129, 1944.
- Ramon Díaz-Uriarte and Sara Alvarez De Andrés. Gene Selection and Classification of Microarray Data using Random Forest. *BMC Bioinformatics*, 7(1):1–13, 2006.
- Jianqing Fan, Yunbei Ma, and Wei Dai. Nonparametric Independence Screening in Sparse Ultra-high-dimensional Varying Coefficient Models. *Journal of the American Statistical Association*, 109(507):1270–1284, 2014.
- Walter D Fisher. On Grouping for Maximum Homogeneity. *Journal of the American statistical Association*, 53(284):789–798, 1958.
- Robin Genuer, Jean-Michel Poggi, and Christine Tuleau-Malot. Variable Selection using Random Forests. *Pattern recognition letters*, 31(14):2225–2236, 2010.
- Léo Grinsztajn, Edouard Oyallon, and Gaël Varoquaux. Why do tree-based models still outperform deep learning on typical tabular data? *Advances in neural information processing systems*, 35:507–520, 2022.
- P Richard Hahn, Jared S Murray, and Carlos M Carvalho. Bayesian Regression Tree Models for Causal Inference: Regularization, Confounding, and Heterogeneous Effects (with discussion). *Bayesian Analysis*, 15(3):965–1056, 2020.
- Trevor Hastie, Robert Tibshirani, Jerome H Friedman, and Jerome H Friedman. *The Elements of Statistical Learning: Data mining, Inference, and Prediction*, volume 2. Springer, 2009.
- Myles Hollander, Douglas A Wolfe, and Eric Chicken. *Nonparametric Statistical Methods*. John Wiley & Sons, 2013.
- Akira Horiguchi, Matthew T Pratola, and Thomas J Santner. Assessing Variable Activity for Bayesian Regression Trees. *Reliability Engineering & System Safety*, 207:107391, 2021.
- Jason M Klusowski and Peter M Tian. Large scale prediction with decision trees. *Journal of the American Statistical Association*, 119(545):525–537, 2024.
- Miron B Kurşa and Witold R Rudnicki. Feature selection with the boruta package. *Journal of Statistical Software*, 36(11):1–13, 2010.
- William La Cava, Patryk Orzechowski, Bogdan Burlacu, Fabrício Olivetti de França, Marco Virgolin, Ying Jin, Michael Kommenda, and Jason H Moore. Contemporary Symbolic Regression Methods and their Relative Performance. *arXiv preprint arXiv:2107.14351*, 2021.
- Michel Ledoux and Michel Talagrand. *Probability in Banach Spaces: isoperimetry and processes*, volume 23. Springer Science & Business Media, 1991.
- Meng Li and Li Ma. Learning Asymmetric and Local Features in Multi-dimensional Data through Wavelets with Recursive Partitioning. *IEEE Transactions on Pattern Analysis and Machine Intelligence*, 44(11):7674–7687, 2021.
- Antonio R Linero. Bayesian Regression Trees for High-dimensional Prediction and Variable Selection. *Journal of the American Statistical Association*, 113(522):626–636, 2018.

- Chuji Luo and Michael J Daniels. Variable Selection Using Bayesian Additive Regression Trees. *arXiv preprint arXiv:2112.13998*, 2021.
- Hengrui Luo and Anna Ma. Frontal Slice Approaches for Tensor Linear Systems. *arXiv preprint arXiv:2408.13547*, 2024.
- Hengrui Luo and Matthew T Pratola. Sharded Bayesian Additive Regression Trees. *arXiv preprint arXiv:2306.00361*, 2023.
- Hengrui Luo, Akira Horiguchi, and Li Ma. Efficient Decision Trees for Tensor Regressions. *arXiv preprint arXiv:2408.01926*, 2024.
- Nour Makke and Sanjay Chawla. Interpretable Scientific Discovery with Symbolic Regression: A Review. *Artificial Intelligence Review*, 57(1):2, 2024.
- Aditya Krishna Menon and Robert C Williamson. Bipartite Ranking: a Risk-theoretic Perspective. *The Journal of Machine Learning Research*, 17(1):6766–6867, 2016.
- DJ Newman, Eli Passow, and Louis Raymon. Piecewise monotone polynomial approximation. *Transactions of the American Mathematical Society*, 172:465–472, 1972.
- J. Ross Quinlan. Induction of decision trees. *Machine learning*, 1:81–106, 1986.
- Veronika Ročková and Enakshi Saha. On theory for BART. In *The 22nd international conference on artificial intelligence and statistics*, pages 2839–2848. PMLR, 2019.
- Veronika Ročková and Stéphanie van der Pas. Posterior Concentration for Bayesian Regression Trees and Forests. *The Annals of Statistics*, 48(4):2108–2131, 2020.
- Omer Ronen, Theo Saarinen, Yan Shuo Tan, James Duncan, and Bin Yu. A mixing time lower bound for a simplified version of bart. *arXiv preprint arXiv:2210.09352*, 2022.
- Erwan Scornet, Gérard Biau, and Jean-Philippe Vert. Consistency of random forests. *The Annals of Statistics*, 43(4):1716–1741, 2015.
- Carolin Strobl, Anne-Laure Boulesteix, Thomas Kneib, Thomas Augustin, and Achim Zeileis. Conditional variable importance for random forests. *BMC Bioinformatics*, 9(1):1–11, 2008.
- Kazuki Uematsu and Yoonkyung Lee. On Theoretically Optimal Ranking Functions in Bipartite Ranking. *Journal of the American Statistical Association*, 112(519):1311–1322, 2017.
- Sara van de Geer. On the uniform convergence of empirical norms and inner products, with application to causal inference. *Electronic Journal of Statistics*, 8(1):543 – 574, 2014.
- Marvin N Wright and Andreas Ziegler. ranger: A fast implementation of random forests for high-dimensional data in c++ and r. *Journal of Statistical Software*, 77:1–17, 2017.
- Shengbin Ye, Thomas P Senftle, and Meng Li. Operator-induced structural variable selection with applications to materials genomes. *Journal of the American Statistical Association*, 119(545): 81–94, 2024.
- Cheng Li Yichen Zhu and David B. Dunson. Classification Trees for Imbalanced Data: Surface-to-Volume Regularization. *Journal of the American Statistical Association*, 118(543):1707–1717, 2023.

Appendices

Appendix A. Proof of Lemma 1

Proof Suppose that $P'_1 = \{y_{(1)} < y_{(2)} < \dots < y_{(i+1)}\}$ and $P'_2 = \{y_{(i)} < y_{(i+2)} < \dots < y_{(n)}\}$ and the variance of P'_1 is strictly smaller than the variance of P_1^{**} , then we can write explicitly that the group means for P'_1 and P'_2 : $\mu'_1 = \frac{1}{i} \cdot (\mu_1^* \cdot i - y_{(i)} + y_{(i+1)})$ and $\mu'_2 = \frac{1}{n-i} \cdot (\mu_2^* \cdot (n-i) - y_{(i+1)} + y_{(i)})$, where μ_1^*, μ_2^* are corresponding in-group means of P_1^*, P_2^* . Since we assume that the variance of P_1^* is strictly smaller than the variance of P_1^{**} , our idea is to prove that switching $y_{(i+1)}$ and $y_{(i)}$ will reduce P'_1 to P_1^* and P'_2 to P_2^* with strictly smaller sum of group variances.

Now, we consider the differences $\mu_1^* - \mu'_1 = \mu_1^* - \frac{1}{i} \cdot (\mu_1^* \cdot i - y_{(i)} + y_{(i+1)}) = -\frac{1}{i} \cdot (-y_{(i)} + y_{(i+1)}) < 0$ and $\mu_2^* - \mu'_2 = \mu_2^* - \frac{1}{n-i} \cdot (\mu_2^* \cdot (n-i) - y_{(i+1)} + y_{(i)}) = -\frac{1}{n-i} \cdot (-y_{(i+1)} + y_{(i)}) > 0$.

$$\begin{aligned}
 & \sum_{y_{(j)} \in P'_1} (y_{(j)} - \mu'_1)^2 + \sum_{y_{(j)} \in P'_2} (y_{(j)} - \mu'_2)^2 \tag{20} \\
 &= \sum_{j=1}^{i-1} (y_{(j)} - \mu'_1)^2 + (y_{(i+1)} - \mu'_1)^2 + (y_{(i)} - \mu'_2)^2 + \sum_{j=i+2}^n (y_{(j)} - \mu'_2)^2 \\
 &= \sum_{j=1}^{i-1} (y_{(j)} - \mu_1^* + \mu_1^* - \mu'_1)^2 + (y_{(i+1)} - \mu_2^* + \mu_2^* - \mu'_2)^2 + (y_{(i)} - \mu_1^* + \mu_1^* - \mu'_2)^2 + \sum_{j=i+2}^n (y_{(j)} - \mu_2^* + \mu_2^* - \mu'_2)^2 \\
 &= \left(\sum_{j=1}^{i-1} (y_{(j)} - \mu_1^*)^2 + \sum_{j=1}^{i-1} 2(y_{(j)} - \mu_1^*)(\mu_1^* - \mu'_1) + \sum_{j=1}^{i-1} (\mu_1^* - \mu'_1)^2 \right) + (y_{(i+1)} - \mu_2^* + \mu_2^* - \mu'_2)^2 \\
 &+ \left(\sum_{j=i+2}^n (y_{(j)} - \mu_2^*)^2 + \sum_{j=i+2}^n 2(y_{(j)} - \mu_2^*)(\mu_2^* - \mu'_2) + \sum_{j=i+2}^n (\mu_2^* - \mu'_2)^2 \right) + (y_{(i)} - \mu_1^* + \mu_1^* - \mu'_2)^2 \\
 &= \left(\sum_{j=1}^{i-1} (y_{(j)} - \mu_1^*)^2 + 2(\mu_1^* - \mu'_1) \sum_{j=1}^{i-1} (y_{(i)} - \mu_1^*) + \sum_{j=1}^{i-1} (\mu_1^* - \mu'_1)^2 \right) + (y_{(i+1)} - \mu_2^*)^2 \\
 &+ 2(y_{(i+1)} - \mu_2^*)(\mu_2^* - \mu'_2) + (\mu_2^* - \mu'_2)^2 \\
 &+ \left(\sum_{j=i+2}^n (y_{(j)} - \mu_2^*)^2 + 2(\mu_2^* - \mu'_2) \sum_{j=1}^{i-1} (y_{(j)} - \mu_2^*) + \sum_{j=i+2}^n (\mu_2^* - \mu'_2)^2 \right) + (y_{(i)} - \mu_1^*)^2 \\
 &+ 2(y_{(i)} - \mu_1^*)(\mu_1^* - \mu'_2) + (\mu_1^* - \mu'_2)^2 \tag{21}
 \end{aligned}$$

$$\begin{aligned}
 &= \sum_{j=1}^i (y_{(j)} - \mu_1^*)^2 + 2(\mu_1^* - \mu'_1) \sum_{j=1}^{i-1} (y_{(i)} - \mu_1^*) + \left[(\mu_2^* - \mu'_2)^2 + \sum_{j=1}^{i-1} (\mu_1^* - \mu'_1)^2 \right] \\
 &+ \sum_{j=i+1}^n (y_{(j)} - \mu_2^*)^2 + 2(\mu_2^* - \mu'_2) \sum_{j=1}^{i-1} (y_{(j)} - \mu_2^*) + \left[(\mu_1^* - \mu'_2)^2 + \sum_{j=i+2}^n (\mu_2^* - \mu'_2)^2 \right] \tag{22}
 \end{aligned}$$

$$\begin{aligned}
 &= \sum_{j=1}^i (y_{(j)} - \mu_1^*)^2 - \frac{2}{i} (-y_{(i)} + y_{(i+1)})^2 + \left[(\mu_2^* - \mu_1')^2 + \sum_{j=1}^{i-1} (\mu_1^* - \mu_1')^2 \right] \\
 &\quad + \sum_{j=i+1}^n (y_{(j)} - \mu_2^*)^2 - \frac{2}{n-i} (-y_{(i+1)} + y_{(i)})^2 + \left[(\mu_1^* - \mu_2')^2 + \sum_{j=i+2}^n (\mu_2^* - \mu_2')^2 \right] \quad (23)
 \end{aligned}$$

We use red and blue colored fonts to show how we group the terms in formula, and note that the red and blue parts are essentially the variances of P_1^* and P_2^* , namely $\sum_{y_{(j)} \in P_1^*} (y_{(j)} - \mu_1^*)^2 + \sum_{y_{(j)} \in P_2^*} (y_{(j)} - \mu_2^*)^2$, and we show below that the rest part is greater than zero. From the assumption (for the last inequality) that $n > 4$, $\min(n-i, i) > 2$, we have

$$\begin{aligned}
 2(\mu_1^* - \mu_1') \sum_{j=1}^{i-1} (y_{(j)} - \mu_1^*) &= 2 \left(-\frac{1}{i} \cdot (-y_{(i)} + y_{(i+1)}) \right) (-y_{(i)} + y_{(i+1)}) \\
 &= -\frac{2}{i} (-y_{(i)} + y_{(i+1)})^2 \geq -(-y_{(i+1)} + y_{(i)})^2 \quad (24)
 \end{aligned}$$

$$\begin{aligned}
 2(\mu_2^* - \mu_2') \sum_{j=1}^{i-1} (y_{(j)} - \mu_2^*) &= 2 \left(-\frac{1}{n-i} \cdot (-y_{(i+1)} + y_{(i)}) \right) (-y_{(i+1)} + y_{(i)}) \\
 &= -\frac{2}{n-i} (-y_{(i+1)} + y_{(i)})^2 \geq -(-y_{(i+1)} + y_{(i)})^2 \quad (25)
 \end{aligned}$$

Now we want to compare $-\frac{2}{i} (-y_{(i)} + y_{(i+1)})^2$ and $(\mu_2^* - \mu_1')^2$. But from the sorted assumption and (24), $\mu_1' \leq y_{(i)} < y_{(i+1)} \leq \mu_2^*$,

$$-\frac{2}{i} (-y_{(i)} + y_{(i+1)})^2 + (\mu_2^* - \mu_1')^2 \geq -(-y_{(i)} + y_{(i+1)})^2 + (\mu_2^* - \mu_1')^2 \geq 0 \quad (26)$$

Similarly, we can compare $-\frac{2}{n-i} (-y_{(i+1)} + y_{(i)})^2$ and $(\mu_1^* - \mu_2')^2$ where we use (25) and $\mu_1^* \leq y_{(i)} < y_{(i+1)} \leq \mu_2'$:

$$-\frac{2}{n-i} (-y_{(i+1)} + y_{(i)})^2 + (\mu_1^* - \mu_2')^2 \geq -(-y_{(i)} + y_{(i+1)})^2 + (\mu_2^* - \mu_1')^2 \geq 0 \quad (27)$$

Using both (26) and (27) in (23), we have proven that

$$\sum_{y_{(j)} \in P_1'} (y_{(j)} - \mu_1')^2 + \sum_{y_{(j)} \in P_2'} (y_{(j)} - \mu_2')^2 \geq \sum_{y_{(j)} \in P_1^*} (y_{(j)} - \mu_1^*)^2 + \sum_{y_{(j)} \in P_2^*} (y_{(j)} - \mu_2^*)^2.$$

This means that switching $y_{(i)}$ and $y_{(i+1)}$ indeed reduces the total in-group variances. For more general situations, given two partitions P_1, P_2 of fixed sizes, and assume $\mu_1 < \mu_2$. We can first sort responses and find any pair of responses (y_α, y_β) such that $y_\alpha \in P_1, y_\beta \in P_2$ and $y_\alpha > y_\beta$. We put y_α into P_2 and y_β into P_1 and repeat the argument above to show that the in-group variances for both partition group decreases.

Similarly, assuming that the variance of P_1^* is strictly larger than the variance of P_1^{**} , we can prove that another global minimum of the loss function is given by assuming partitions of P_1^{**} and P_2^{**} . The key observation is that, the loss can be considered as a function of two sets P_1', P_2' and there are two local minima attained by P_1^*, P_2^* or P_1^{**}, P_2^{**} . The above arguments only prove that P_1^*, P_2^* and P_1^{**}, P_2^{**} both attain local minima, and they are the only possible local minima. ■

Appendix B. Proof of Proposition 7

Proof Without loss of generality, we assume that the LHS takes the ordered form $\sum_{i=1}^{n_{\text{left}}} (y_{(i)} - \mu_L^{C,k})^2 + \sum_{i=n_{\text{left}}+1}^n (y_{(i)} - \mu_R^{C,k})^2$ where n_{left} is the number of observations in the left node.

$$\begin{aligned}
 \sum_{i=1}^n (y_{(i)} - \mu^\#)^2 &= \sum_{i=1}^{n_{\text{left}}} (y_{(i)} - \mu^\#)^2 + \sum_{i=n_{\text{left}}+1}^n (y_{(i)} - \mu^\#)^2 \\
 &= \sum_{i=1}^{n_{\text{left}}} (y_{(i)} - \mu_L^{C,k} + \mu_L^{C,k} - \mu^\#)^2 + \sum_{i=n_{\text{left}}+1}^n (y_{(i)} - \mu_R^{C,k} + \mu_R^{C,k} - \mu^\#)^2 \\
 &= \sum_{i=1}^{n_{\text{left}}} (y_{(i)} - \mu_L^{C,k})^2 + \sum_{i=n_{\text{left}}+1}^n (y_{(i)} - \mu_R^{C,k})^2 + \sum_{i=1}^{n_{\text{left}}} (\mu_L^{C,k} - \mu^\#)^2 + \sum_{i=n_{\text{left}}+1}^n (\mu_R^{C,k} - \mu^\#)^2 \\
 &\quad + 2 \underbrace{\sum_{i=1}^{n_{\text{left}}} (y_{(i)} - \mu_L^{C,k})(\mu_L^{C,k} - \mu^\#)}_{=0} + 2 \underbrace{\sum_{i=n_{\text{left}}+1}^n (y_{(i)} - \mu_R^{C,k})(\mu_R^{C,k} - \mu^\#)}_{=0} \\
 &= \sum_{i=1}^{n_{\text{left}}} (y_{(i)} - \mu_L^{C,k})^2 + \sum_{i=n_{\text{left}}+1}^n (y_{(i)} - \mu_R^{C,k})^2 + \sum_{i=1}^{n_{\text{left}}} (\mu_L^{C,k} - \mu^\#)^2 + \sum_{i=n_{\text{left}}+1}^n (\mu_R^{C,k} - \mu^\#)^2
 \end{aligned}$$

We attained the desired inequality by dropping the third and fourth summation in the last equality. \blacksquare

Appendix C. Proof of Proposition 8

Proof As the statement of the proposition, we can consider three cases as follows, with an illustrative reference to Figure 3. The corresponding three cases for (1) both of them have 0 pre-image (2) both of them have 1 pre-image (3) one of them have 0 pre-image and the other has 1 pre-image, are detailed as follows:

1. θ_1 has 0 pre-image of C_1 on I ; θ_2 has 0 pre-image of C_2 on I . Then, on the refined interval $I \in \mathcal{I}_{1 \cap 2}$, either $\theta_1(u) \leq C_1$ or $\theta_1(u) > C_1$, for $\forall u \in I$. Note that pre-image is well-defined when the θ_1 (and θ_2) is restricted on a refined interval $I \in \mathcal{I}_{1 \cap 2}$. This indicates that over I the splitting value corresponding to $\theta_1^{-1}(C_1)$ will not separate any $\mathbf{x}_k \in I$. Similarly, the splitting value for \mathbf{x} corresponding to $\theta_2^{-1}(C_2)$ will not separate any univariate inputs $x_k \in I$. The corresponding terms in the principal decision ratios 9 becomes:

$$\begin{aligned}
 \tau|_I &= \frac{\exp(-\sum_{i=1}^n (y_i - \mu_L^1)^2 \mathbf{1}(z_{i,k_1} \leq C_1) \mathbf{1}(\mathbf{x}_{i,k_1} \in I) - \sum_{i=1}^n (y_i - \mu_R^1)^2 \mathbf{1}(z_{i,k_1} > C_1) \mathbf{1}(\mathbf{x}_{i,k_1} \in I))}{\exp(-\sum_{i=1}^n (y_i - \mu_L^2)^2 \mathbf{1}(z_{i,k_2} \leq C_2) \mathbf{1}(\mathbf{x}_{i,k_2} \in I) - \sum_{i=1}^n (y_i - \mu_R^2)^2 \mathbf{1}(z_{i,k_2} > C_2) \mathbf{1}(\mathbf{x}_{i,k_2} \in I))} \quad (28) \\
 &= \frac{\exp(-\sum_{i=1}^{n_1} (y_{(i)} - \mu_L^1)^2 \mathbf{1}(z_{(i),k_1} \leq C_1) \mathbf{1}(\mathbf{x}_{(i),k_1} \in I) - \sum_{i=n_1+1}^n (y_{(i)} - \mu_R^1)^2 \mathbf{1}(z_{(i),k_1} > C_1) \mathbf{1}(\mathbf{x}_{(i),k_1} \in I))}{\exp(-\sum_{i=1}^{n_2} (y_{(i)} - \mu_L^2)^2 \mathbf{1}(z_{(i),k_2} \leq C_2) \mathbf{1}(\mathbf{x}_{(i),k_2} \in I) - \sum_{i=n_2+1}^n (y_{(i)} - \mu_R^2)^2 \mathbf{1}(z_{(i),k_2} > C_2) \mathbf{1}(\mathbf{x}_{(i),k_2} \in I))} \quad (29)
 \end{aligned}$$

Since there are 0 pre-images for θ_1 over I , either $\mathbf{1}(z_{i,k_1} \leq C_1) \mathbf{1}(\mathbf{x}_{i,k_1} \in I) \equiv 0$ or $\mathbf{1}(z_{i,k_1} > C_1) \mathbf{1}(\mathbf{x}_{i,k_1} \in I) \equiv 0$; similarly since there are 0 pre-images for θ_2 over I , either $\mathbf{1}(z_{i,k_2} \leq C_2) \mathbf{1}(\mathbf{x}_{i,k_2} \in I) \equiv 0$ or $\mathbf{1}(z_{i,k_2} > C_2) \mathbf{1}(\mathbf{x}_{i,k_2} \in I) \equiv 0$. In the case $\mathbf{1}(z_{i,k_1} \leq C_1) \mathbf{1}(\mathbf{x}_{i,k_1} \in I) \equiv 0$

and $\mathbf{1}(z_{i,k_2} \leq C_2)\mathbf{1}(x_{i,k_2} \in I) \equiv 0$, 29 becomes

$$\begin{aligned} \tau |_I &= \frac{\exp\left(-\sum_{i=n_1+1}^n (y_{(i)} - \mu_R^1)^2 \mathbf{1}(z_{(i),k_1} > C_1)\mathbf{1}(x_{(i),k_1} \in I)\right)}{\exp\left(-\sum_{i=n_2+1}^n (y_{(i)} - \mu_R^2)^2 \mathbf{1}(z_{(i),k_2} > C_2)\mathbf{1}(x_{(i),k_2} \in I)\right)} \\ &= \frac{\exp\left(-\sum_{i=1}^n (y_{(i)} - \mu_R^1)^2\right)}{\exp\left(-\sum_{i=1}^n (y_{(i)} - \mu_R^2)^2\right)} \\ &= \frac{\exp\left(-\sum_{i=1}^n (y_i - \mu_R^1)^2\right)}{\exp\left(-\sum_{i=1}^n (y_i - \mu_R^2)^2\right)} \\ &= 1 \text{ by definition, } \mu_R^1 = \mu_R^2. \end{aligned}$$

The case $\mathbf{1}(z_{i,k_1} > C_1)\mathbf{1}(x_{i,k_1} \in I) \equiv 0$ and $\mathbf{1}(z_{i,k_2} > C_2)\mathbf{1}(x_{i,k_2} \in I) \equiv 0$ follows the same argument. In the case $\mathbf{1}(z_{i,k_1} \leq C_1)\mathbf{1}(x_{i,k_1} \in I) \equiv 0$ and $\mathbf{1}(z_{i,k_2} > C_2)\mathbf{1}(x_{i,k_2} \in I) \equiv 0$ we have

$$\begin{aligned} \tau |_I &= \frac{\exp\left(-\sum_{i=n_1+1}^n (y_{(i)} - \mu_R^1)^2 \mathbf{1}(z_{(i),k_1} > C_1)\mathbf{1}(x_{(i),k_1} \in I)\right)}{\exp\left(-\sum_{i=1}^{n_2} (y_{(i)} - \mu_L^2)^2 \mathbf{1}(z_{(i),k_2} \leq C_2)\mathbf{1}(x_{(i),k_2} \in I)\right)} \\ &= \frac{\exp\left(-\sum_{i=1}^n (y_{(i)} - \mu_R^1)^2\right)}{\exp\left(-\sum_{i=1}^n (y_{(i)} - \mu_L^2)^2\right)} \\ &= \frac{\exp\left(-\sum_{i=1}^n (y_i - \mu_R^1)^2\right)}{\exp\left(-\sum_{i=1}^n (y_i - \mu_L^2)^2\right)} \\ &= 1 \text{ by definition, } \mu_R^1 = \mu_L^2. \end{aligned}$$

Note that this case we also have all observations allocated to right and left nodes under two transforms. The case $\mathbf{1}(z_{i,k_1} > C_1)\mathbf{1}(x_{i,k_1} \in I) \equiv 0$ and $\mathbf{1}(z_{(i),k_2} \leq C_2)\mathbf{1}(x_{i,k_2} \in I) \equiv 0$ follows the same argument.

2. θ_1 has 1 pre-image of C_1 on I ; θ_2 has 0 pre-image of C_2 on I . (The discussion of the case: θ_1 has 0 pre-image of C_1 on I ; θ_2 has 1 pre-image of C_2 on I , is similar.) First note that $\mu_L^2 = \mu_R^2$ as θ_2 has 0 pre-image but $\mu_L^1 \neq \mu_R^1$, yielding that the corresponding principal decision ratios:

$$\begin{aligned} \tau |_I &= \frac{\exp\left(-\sum_{i=1}^n (y_{(i)} - \mu_L^1)^2 \mathbf{1}(z_{(i),k_1} \leq C_1)\mathbf{1}(x_{(i),k_1} \in I) - \sum_{i=1}^n (y_{(i)} - \mu_R^1)^2 \mathbf{1}(z_{(i),k_1} > C_1)\mathbf{1}(x_{(i),k_1} \in I)\right)}{\exp\left(-\sum_{i=1}^n (y_{(i)} - \mu_L^2)^2 \mathbf{1}(z_{(i),k_2} \leq C_2)\mathbf{1}(x_{(i),k_2} \in I)\right)}, \\ \text{or } & \frac{\exp\left(-\sum_{i=1}^n (y_{(i)} - \mu_L^1)^2 \mathbf{1}(z_{(i),k_1} \leq C_1) - \sum_{i=1}^n (y_{(i)} - \mu_R^1)^2 \mathbf{1}(z_{(i),k_1} > C_1)\mathbf{1}(x_{(i),k_1} \in I)\right)}{\exp\left(-\sum_{i=1}^n (y_{(i)} - \mu_R^2)^2 \mathbf{1}(z_{(i),k_2} > C_2)\mathbf{1}(x_{(i),k_2} \in I)\right)}. \end{aligned}$$

Therefore, the ratio is larger for θ_1 by Proposition 7 and we should always prefer θ_1 because the fit for (x, y) using two constants $\mu_L^1 \cdot \mathbf{1}(z_{(i),k_1} \leq C_1)$ and $\mu_R^1 \cdot \mathbf{1}(z_{(i),k_1} > C_1)$ defined on I can not be worse than the fit for (x, y) using one constant $\mu_L^2 \cdot \mathbf{1}(z_{(i),k_2} \leq C_2)$ (or $\mu_R^2 \cdot \mathbf{1}(z_{(i),k_2} > C_2)$), as stated in the next Proposition 7.

3. θ_1 has 1 pre-image of C_1 on I ; θ_2 has 1 pre-image of C_2 on I . Then, on the refined interval $I \in \mathcal{I}_{1 \cap 2}$, 29 becomes

$$\tau |_I = \frac{\exp\left(-\sum_{i=1}^{n_1} (y_{(i)} - \mu_L^1)^2 \mathbf{1}(x_{(i),k_1} \leq \theta_1^{-1}C_1)\mathbf{1}(x_{(i),k_1} \in I) - \sum_{i=n_1+1}^n (y_{(i)} - \mu_R^1)^2 \mathbf{1}(x_{(i),k_1} > \theta_1^{-1}C_1)\mathbf{1}(x_{(i),k_1} \in I)\right)}{\exp\left(-\sum_{i=1}^{n_2} (y_{(i)} - \mu_L^2)^2 \mathbf{1}(x_{(i),k_2} \leq \theta_2^{-1}C_2)\mathbf{1}(x_{(i),k_2} \in I) - \sum_{i=n_2+1}^n (y_{(i)} - \mu_R^2)^2 \mathbf{1}(x_{(i),k_2} > \theta_2^{-1}C_2)\mathbf{1}(x_{(i),k_2} \in I)\right)}$$

From Corollary 4, we know that both the numerator and denominator of $\tau |_I$ are fixed size oracle 2-partitions on y . However, we need to decide which of $x_{(i),k_1} \leq \theta_1^{-1}C_1$ and $x_{(i),k_2} \leq \theta_2^{-1}C_2$ gives us a larger sum of variances. From Lemma 15, we know that it reduces to compare $n - 1$ possible values of sum of variances (corresponding to $n - 1$ different split values).

■

Appendix D. Proof of Theorem 10

Proof Using Theorem 3 in Cossock and Zhang (2006), we know that for the full dataset $\mathcal{X}^{(N)}$, the following holds:

$$\mathbf{T}(r_B) - \mathbf{T}(r_{c,K}) \leq \frac{4}{\sqrt{N}} \left(\sum_{j=1}^N (f_B(\mathbf{x}_j) - f_{c,K}(\mathbf{x}_j))^2 \right)^{1/2}, \quad (30)$$

where $r_{c,K}$ is induced by the $f_{c,K} \in \mathcal{G} \subset \mathcal{G}_0$ constructed from a CART. This inequality suggests that the a scoring function $f_{c,K}$ approximated by CART of depth $K \geq 1$ with low approximating L_2 error to the Bayes scoring function f_B can attain low approximating ranking error \mathbf{T} as well.

Assuming that the true signal $f_B \in \mathcal{G}_0$ and the CART-induced $f_{c,K} \in \mathcal{G} \subset \mathcal{G}_0$ as in the statement of Theorem 10, now we apply Theorem 4.3 in Klusowski and Tian (2024). We can assert that the CART prediction $f_{c,K}$ constructed from splitting a complete binary tree using CART loss (10) of depth K satisfy the following universal consistency as:

$$\mathbb{E}_{(\mathcal{X}^{(N)}, \mathcal{Y}^{(N)})} \left(\|f_B - f_{c,K}\|^2 \right) \leq 2 \inf_{g \in \mathcal{G}} \left\{ \|f_B - g\|^2 + \frac{\|g\|_{\text{TV}}^2}{K+3} + C_B \frac{2^K \log(Nd)}{N} \right\}, \quad (31)$$

where the constant C_B depends on the uniform bound on the total variations along coordinates $f_{B,i} : \mathbb{R} \rightarrow \mathbb{R}$ as assumed. Applying Markov's inequality yields

$$\mathbb{P}_{(\mathcal{X}^{(N)}, \mathcal{Y}^{(N)})} \left(\|f_B - f_{c,K}\|^2 > \alpha_1 \right) \leq \frac{\mathbb{E}_{(\mathcal{X}^{(N)}, \mathcal{Y}^{(N)})} \left(\|f_B - f_{c,K}\|^2 \right)}{\alpha_1} \quad (32)$$

$$\leq \frac{2}{\alpha_1} \inf_{g \in \mathcal{G}} \left\{ \|f_B - g\|^2 + \frac{\|g\|_{\text{TV}}^2}{K+3} + C_B \frac{2^K \log^2 N \log(Nd)}{N} \right\}, \quad (33)$$

for any $\alpha_1 > 0$. This means that the tree-like functions in class \mathcal{G} can approximate the Bayes score function well enough, and bounded from above.

Since the result in (33) considers the exact norm, we need one more step to connect the exact norm to the empirical norm used in the statement of Theorem 3 in Cossock and Zhang (2006). To attain this, we invoke classical results from empirical process regarding the convergence of empirical norm (Ledoux and Talagrand, 1991). According to Theorem 2.2 in van de Geer (2014), the empirical norm $\|f\|_N^2 := \frac{1}{N} \sum_{i=1}^N f(\mathbf{x}_i)^2$ converges to the exact ℓ^2 -norm $\|f\|^2 = \int f(u)^2 d\mathbb{P}_X(u)$ at a rate of $\mathcal{O}\left(\frac{1}{\sqrt{N}}\right)$ for any $f \in \mathcal{G}_0$ from a possibly larger class than tree-like functions \mathcal{G} . In particular, we have that the empirical norm of $f \in \mathcal{G}_0$ can be approximated as well

$$\mathbb{E}_{(\mathcal{X}^{(N)}, \mathcal{Y}^{(N)})} \left(\sup_{f \in \mathcal{G}_0} \left| \|f\|_N - \|f\| \right| \right) \leq \frac{2R_\infty J_0(2R_2, \mathcal{G}_0)}{\sqrt{N}}, \quad (34)$$

which implies

$$\mathbb{P}_{(\mathcal{X}^{(N)}, \mathcal{Y}^{(N)})} \left(\sup_{f \in \mathcal{G}_0} \left| \|f\|_N - \|f\| \right| > \alpha_2 \right) \leq \frac{\mathbb{E}_{(\mathcal{X}^{(N)}, \mathcal{Y}^{(N)})} \left(\sup_{f \in \mathcal{G}_0} \left| \|f\|_N - \|f\| \right| \right)}{\alpha_2} \quad (35)$$

$$\leq \frac{2R_\infty J_0(2R_2, \mathcal{G}_0)}{\alpha_2 \sqrt{N}}, \quad (36)$$

for any $\alpha_2 > 0$ by applying Markov's inequality. Applying the inequality in (30), we obtain

$$\begin{aligned}
 & \mathbb{P}_{(\mathcal{X}^{(N)}, \mathcal{Y}^{(N)})} (\mathbf{T}(r_B) - \mathbf{T}(r_{c,K}) > \varepsilon_N) \\
 & \leq \mathbb{P}_{(\mathcal{X}^{(N)}, \mathcal{Y}^{(N)})} \left(\frac{4}{\sqrt{N}} \left(\sum_{j=1}^N (f_B(\mathbf{x}_j) - f_{c,K}(\mathbf{x}_j))^2 \right)^{1/2} > \varepsilon_N \right) \\
 & = \mathbb{P}_{(\mathcal{X}^{(N)}, \mathcal{Y}^{(N)})} \left(\frac{1}{N} \left(\sum_{j=1}^N (f_B(\mathbf{x}_j) - f_{c,K}(\mathbf{x}_j))^2 \right) > \frac{\varepsilon_N^2}{16} \right) \\
 & = \mathbb{P}_{(\mathcal{X}^{(N)}, \mathcal{Y}^{(N)})} \left(\|f_{c,K} - f_B\|_N > \frac{\varepsilon_N^2}{16} \text{ and } \left| \|f_{c,K} - f_B\|_N - \|f_{c,K} - f_B\| \right| \leq \frac{\varepsilon_N^2}{32} \right) \\
 & \quad + \mathbb{P}_{(\mathcal{X}^{(N)}, \mathcal{Y}^{(N)})} \left(\|f_{c,K} - f_B\|_N > \frac{\varepsilon_N^2}{16} \text{ and } \left| \|f_{c,K} - f_B\|_N - \|f_{c,K} - f_B\| \right| > \frac{\varepsilon_N^2}{32} \right) \\
 & =: A_1 + A_2. \tag{37}
 \end{aligned}$$

For the first term A_1 , it represents how well the tree-like function class \mathcal{G} can approximate the Bayes scoring functions. We substitute $\alpha_1 = \frac{\varepsilon_N^2}{32}$ into (33) and bound it by

$$\mathbb{P}_{(\mathcal{X}^{(N)}, \mathcal{Y}^{(N)})} \left(\|f_B - f_{c,K}\|^2 > \left[\frac{\varepsilon_N^2}{32} \right]^2 \right) \leq \frac{1024}{\varepsilon_N^4} \cdot \inf_{g \in \mathcal{G}} \left\{ \|f_B - g\|^2 + \frac{\|g\|_{\text{TV}}^2}{K+3} + C_B \frac{2^K \log^2 N \log(Nd)}{N} \right\}.$$

For the second term A_2 , it represents how fast empirical norm with respect to \mathbf{X} converges when the Bayesian scoring function is in a potentially larger class \mathcal{G}_0 (but the tree approximating scoring function $f_{c,K} \in \mathcal{G}$). This enclosed event has an intersection component in form of (36) with $\alpha_2 = \frac{\varepsilon_N^2}{16}$. Therefore, $A_2 \leq \frac{32R_\infty J_0(2R_2, \mathcal{G}_0)}{\varepsilon_N^2 \sqrt{N}}$.

Combining these two bounds yields

$$\begin{aligned}
 & \mathbb{P}_{(\mathcal{X}^{(N)}, \mathcal{Y}^{(N)})} (\mathbf{T}(r_B) - \mathbf{T}(r_{c,K}) > \varepsilon_N) \\
 & \leq \frac{1024}{\varepsilon_N^4} \cdot \inf_{g \in \mathcal{G}} \left\{ \|f_B - g\|^2 + \frac{\|g\|_{\text{TV}}^2}{K+3} + C_B \frac{2^K \log^2 N \log(Nd)}{N} \right\} + \frac{32R_\infty J_0(2R_2, \mathcal{G}_0)}{\varepsilon_N^2 \sqrt{N}}.
 \end{aligned}$$

This completes the proof of the inequality (16).

When $\mathcal{G}_0 = \mathcal{G}$, substituting $g = f_B$ into the upper bound (16) leads to the simplified upper bound (17). ■

Appendix E. Proof of Theorem 13

Proof Using Theorem 3 in Cossock and Zhang (2006), we know that for the full dataset $\mathcal{X}^{(N)}$ we have the bound

$$\mathbf{T}(r_B) - \mathbf{T}(r_f) \leq \frac{4}{\sqrt{N}} \left(\sum_{j=1}^N (f_B(\mathbf{x}_j) - f(\mathbf{x}_j))^2 \right)^{1/2} \tag{38}$$

Therefore, it justifies that the a scoring function f with low approximating L_2 error to the Bayes scoring function f_B can attain low approximating ranking error \mathbf{T} as well.

Ročková and Saha (2019) presents the posterior concentration of BART in their Theorem 7.1 (adapted to our notations above). Namely, when the f is ν -Holder continuous with $0 < \nu \leq 1$ and $\|f_B\|_\infty \lesssim \log^{1/2} N$, assume a regular design $\mathcal{X}^{(N)} = \{\mathbf{x}_1, \mathbf{x}_2, \dots, \mathbf{x}_N\} \subset \mathbb{R}^d, d \lesssim \log^{1/2} N$ for the features. With a fixed number of trees and node η splitting probability $p_{\text{split}}(\eta) = \alpha^{\text{depth}(\eta)}, \alpha \in [\frac{1}{N}, \frac{1}{2})$ proportional to the depth of node η with respect to each tree, we have posterior concentration results from BART, when the regression aims at approximating the optimal f_B . Precisely we assert that the BART posterior measure $\Pi(\cdot | y_1, y_2, \dots, y_N)$ concentrates on all scoring functions f that is measurable with respect to the product σ -field \mathcal{F} generated by the joint measure of y_1, y_2, \dots, y_N . That is, when the approximating scoring function f is approximated by BART, we have

$$\prod (f \in \mathcal{F} : \|f(\mathbf{x}) - f_B(\mathbf{x})\|_N > M_N \varepsilon_N | y_1, y_2, \dots, y_N) \rightarrow 0, \text{ as } N \rightarrow \infty \text{ for all } \mathbf{x} \in \mathcal{X}^{(N)}$$

for any sequence $M_N \rightarrow 0$ in the joint probability of y_1, y_2, \dots, y_N , as the sample size N and the dimensionality $d \rightarrow \infty$ and $\varepsilon_N = N^{-\alpha/(2\alpha+d)} \log^{1/2} N$. Here we use the empirical norm definition $\|f\|_N^2 := \frac{1}{N} \sum_{i=1}^N f(\mathbf{x}_i)^2$ and (38) in the second line.

$$\begin{aligned} & \prod (f \in \mathcal{F} : \mathbf{T}(r_B) - \mathbf{T}(r_f) > M_N \varepsilon_N | y_1, y_2, \dots, y_N) \\ & \leq \prod \left(f \in \mathcal{F} : \frac{4}{\sqrt{N}} \left(\sum_{j=1}^N (f_B(\mathbf{x}_j) - f(\mathbf{x}_j))^2 \right)^{1/2} > M_N \varepsilon_N \middle| y_1, y_2, \dots, y_N \right) \\ & = \prod \left(f \in \mathcal{F} : \frac{1}{N} \left(\sum_{j=1}^N (f_B(\mathbf{x}_j) - f(\mathbf{x}_j))^2 \right) > \frac{M_N^2 \varepsilon_N^2}{16} \middle| y_1, y_2, \dots, y_N \right) \\ & = \prod (f \in \mathcal{F} : \|f - f_B\|_N > M_N^\sharp \varepsilon_N | y_1, y_2, \dots, y_N) \rightarrow 0, \text{ as the design size } N \rightarrow \infty. \end{aligned}$$

where $M_N^\sharp = \frac{M_N^2 \varepsilon_N}{16}$ can be chosen to be any sequence converging to 0 as $N \rightarrow \infty$. The key of this argument is to convert the error measured in \mathbf{T} metric to the empirical norm. \blacksquare

Appendix F. Proof of Lemma 15

Proof Either swapping (y_α, y_γ) or (y_β, y_γ) leaves us with no reversed pairs. Thus, it suffices to note that if we swap (y_α, y_γ) the RHS of (26) and (27) become

$$-(-y_\gamma + y_\alpha)^2 + (\mu_{2,(\alpha,\gamma)}^* - \mu_1')^2 \geq 0,$$

where the $\mu_1' = \frac{1}{n_1} (y_\alpha + y_\beta + \sum_{y \in P_1, y \neq y_\alpha, y_\beta} y)$ and $\mu_{2,(\alpha,\gamma)}^* = \frac{1}{n_2} (y_\alpha + \sum_{y \in P_2, y \neq y_\gamma} y)$. Similarly, if we swap (y_β, y_γ) the RHS of (26) and (27) become

$$-(-y_\gamma + y_\beta)^2 + (\mu_{2,(\beta,\gamma)}^* - \mu_1')^2 \geq 0,$$

where the $\mu_1' = \frac{1}{n_1} (y_\alpha + y_\beta + \sum_{y \in P_1, y \neq y_\alpha, y_\beta} y)$ and $\mu_{2,(\beta,\gamma)}^* = \frac{1}{n_2} (y_\beta + \sum_{y \in P_2, y \neq y_\gamma} y)$. It follows that $\mu_{2,(\alpha,\gamma)}^* > \mu_{2,(\beta,\gamma)}^* > \mu_1'$, and the assumption $y_\alpha > y_\beta > y_\gamma$ that

$$\begin{aligned} & -(-y_\gamma + y_\alpha)^2 + (\mu_{2,(\alpha,\gamma)}^* - \mu_1')^2 + (-y_\gamma + y_\beta)^2 - (\mu_{2,(\beta,\gamma)}^* - \mu_1')^2 \\ & = [(-y_\gamma + y_\beta)^2 - (-y_\gamma + y_\alpha)^2] + [(\mu_{2,(\alpha,\gamma)}^* - \mu_1')^2 - (\mu_{2,(\beta,\gamma)}^* - \mu_1')^2] \geq 0. \end{aligned}$$

This means that the reduction (24)+(25) is larger if we swap (y_α, y_γ) . ■

Appendix G. Proof of Proposition 18

Proof The statistics $\mathcal{T}_0(g)$ in (18) can be written as

$$\sum_{\pi} \left\{ \mathbf{1}(\mathbf{x}_{\pi(1)} \geq \mathbf{x}_{\pi(2)}) \cdot |y_{\pi(1)} - y_{\pi(2)}| \cdot \mathbf{1}(y_{\pi(1)} < y_{\pi(2)}) + \mathbf{1}(\mathbf{x}_{\pi(1)} < \mathbf{x}_{\pi(2)}) \cdot |y_{\pi(1)} - y_{\pi(2)}| \cdot \mathbf{1}(y_{\pi(1)} \geq y_{\pi(2)}) \right\}.$$

Without loss of generality, we next consider one summation involving $\mathbf{1}(f(\mathbf{x}_{\pi(1)}) \geq f(\mathbf{x}_{\pi(2)}))$, and the argument remains the same for the other summation. Now since $\mathbf{X}_k, k \in \{1, \dots, d\}$ is inactive, the distribution of y is independent of the distribution of $f(\mathbf{X}_k)$. Based on this observation, we can remove the conditioning inside the expectation with respect to \mathbf{X}_k in the first line:

$$\begin{aligned} \mathbb{E}_{\mathbf{X}_k, \mathbf{y}} \mathcal{T}_0(g) &= \frac{2}{n(n-1)} \cdot [\mathbb{P}_{\mathbf{X}_k}(f(\mathbf{x}_{\pi(1)}) \geq f(\mathbf{x}_{\pi(2)}))] \cdot \sum_{\pi} [\mathbb{E}_{\mathbf{y}|\mathbf{X}_k} |y_{\pi(1)} - y_{\pi(2)}| \cdot \mathbf{1}(y_{\pi(1)} < y_{\pi(2)})] \\ &= \frac{2}{n(n-1)} \cdot [\mathbb{P}_{\mathbf{X}_k}(f(\mathbf{x}_{\pi(1)}) \geq f(\mathbf{x}_{\pi(2)}))] \cdot \sum_{\pi} [\mathbb{E}_{\mathbf{y}} |y_{\pi(1)} - y_{\pi(2)}| \cdot \mathbf{1}(y_{\pi(1)} < y_{\pi(2)})] \\ &= [\mathbb{P}_{\mathbf{X}_k}(f(\mathbf{x}_{\pi(1)}) \geq f(\mathbf{x}_{\pi(2)}))] \cdot \frac{2}{n(n-1)} \cdot \frac{1}{2} \sum_{\pi} [\mathbb{E}_{\mathbf{y}} |y_{\pi(1)} - y_{\pi(2)}|] \\ &\asymp O(1) \cdot [\mathbb{P}_{\mathbf{X}_k}(f(\mathbf{x}_{\pi(1)}) \geq f(\mathbf{x}_{\pi(2)}))] > 0, \end{aligned}$$

where the second-to-last line uses an symmetric argument as

$$\sum_{\pi} [\mathbb{E}_{\mathbf{y}} |y_{\pi(1)} - y_{\pi(2)}| \cdot \mathbf{1}(y_{\pi(1)} < y_{\pi(2)})] = \sum_{\pi} [\mathbb{E}_{\mathbf{y}} |y_{\pi(1)} - y_{\pi(2)}| \cdot \mathbf{1}(y_{\pi(1)} > y_{\pi(2)})],$$

and their sum is $\sum_{\pi} [\mathbb{E}_{\mathbf{y}} |y_{\pi(1)} - y_{\pi(2)}|]$. This proves part (i).

On the other hand, if we take the expectation with respect to all $\mathbf{y} | \mathbf{X}$:

$$\begin{aligned} \mathbb{E}_{\mathbf{X}, \mathbf{y}} \mathcal{T}_0(g) &= \frac{2}{n(n-1)} \cdot \mathbb{E}_{\mathbf{X}, \mathbf{y}} \sum_{\pi} \mathbf{1}(f(\mathbf{x}_{\pi(1)}) \geq f(\mathbf{x}_{\pi(2)})) \cdot |y_{\pi(1)} - y_{\pi(2)}| \cdot \mathbf{1}(y_{\pi(1)} < y_{\pi(2)}) \\ &= \frac{2}{n(n-1)} \cdot \mathbb{E}_{\mathbf{X}} \mathbb{E}_{\mathbf{y}|\mathbf{X}} \sum_{\pi} \mathbf{1}(f(\mathbf{x}_{\pi(1)}) \geq f(\mathbf{x}_{\pi(2)})) \cdot |y_{\pi(1)} - y_{\pi(2)}| \cdot \mathbf{1}(y_{\pi(1)} < y_{\pi(2)}) \\ &= \frac{2}{n(n-1)} \cdot [\mathbb{E}_{\mathbf{X}} \mathbf{1}(f(\mathbf{x}_{\pi(1)}) \geq f(\mathbf{x}_{\pi(2)}))] \cdot \sum_{\pi} [\mathbb{E}_{\mathbf{y}|\mathbf{X}} |y_{\pi(1)} - y_{\pi(2)}| \cdot \mathbf{1}(y_{\pi(1)} < y_{\pi(2)})] \\ &= \frac{2}{n(n-1)} \cdot [\mathbb{P}_{\mathbf{X}}(f(\mathbf{x}_{\pi(1)}) \geq f(\mathbf{x}_{\pi(2)}))] \cdot \sum_{\pi} [\mathbb{E}_{\mathbf{y}|\mathbf{X}} |y_{\pi(1)} - y_{\pi(2)}| \cdot \mathbf{1}(y_{\pi(1)} < y_{\pi(2)})]. \end{aligned} \tag{39}$$

if there exists such a g that $g(\mathbf{x}_1) \geq g(\mathbf{x}_2) \Leftrightarrow y_1 \geq y_2$ then

$$\begin{aligned}
 (39) &= [\mathbb{P}_{\mathbf{X}} (g(\mathbf{x}_{\pi(1)}) \geq g(\mathbf{x}_{\pi(2)}))] \cdot \sum_{\pi} \frac{2}{n(n-1)} \cdot [\mathbb{E}_{\mathbf{y}|\mathbf{X}} |y_{\pi(1)} - y_{\pi(2)}| \cdot \mathbf{1}(g(\mathbf{x}_{\pi(1)}) < g(\mathbf{x}_{\pi(2)}))] \\
 &= [\mathbb{P}_{\mathbf{X}} (g(\mathbf{x}_{\pi(1)}) \geq g(\mathbf{x}_{\pi(2)}))] \cdot \sum_{\pi} \frac{2}{n(n-1)} \cdot [\mathbb{E}_{\mathbf{y}|\mathbf{X}} (y_{\pi(2)} - y_{\pi(1)}) \cdot \mathbf{1}(g(\mathbf{x}_{\pi(1)}) < g(\mathbf{x}_{\pi(2)}))] \\
 &= [\mathbb{P}_{\mathbf{X}} (g(\mathbf{x}_{\pi(1)}) \geq g(\mathbf{x}_{\pi(2)}))] \cdot \frac{2}{n(n-1)} \\
 &\quad \times \left\{ \sum_{\pi} \mathbb{E}_{\mathbf{y}|\mathbf{X}} y_{\pi(2)} \cdot \mathbf{1}(g(\mathbf{x}_{\pi(1)}) < g(\mathbf{x}_{\pi(2)})) - \sum_{\pi} \mathbb{E}_{\mathbf{y}|\mathbf{X}} y_{\pi(1)} \cdot \mathbf{1}(g(\mathbf{x}_{\pi(1)}) < g(\mathbf{x}_{\pi(2)})) \right\}
 \end{aligned}$$

For the other summation we have equal value $\sum_{\pi} \mathbb{E}_{\mathbf{y}|\mathbf{X}} y_{\pi(2)} \cdot \mathbf{1}(g(\mathbf{x}_{\pi(1)}) \geq g(\mathbf{x}_{\pi(2)})) - \sum_{\pi} \mathbb{E}_{\mathbf{y}|\mathbf{X}} y_{\pi(1)} \cdot \mathbf{1}(g(\mathbf{x}_{\pi(1)}) \geq g(\mathbf{x}_{\pi(2)}))$ and cancels out the last row of expressions. This proves part (ii). \blacksquare